Volume 62

PHYSICA MACEDONICA

A JOURNAL OF EXPERIMENTAL AND
THEORETICAL PHYSICS

INSTITUTE OF PHYSICS

Skopje 2016

ISSN 1409-7168

PHYSICA MACEDONICA

Institute of Physics
Faculty of Natural Sciences and Mathematics
Sts. Cyril and Methodius University,
Skopje, Macedonia

АДРЕСА:
Природно-математички факултет,
Институт за физика,
Гази Баба бб, Пошт. фах 162,
1000 Скопје, Република Македонија

ADRESS:
Sts. Cyril and Methodius University,
Faculty of Natural Sciences and Mathematics, Institute of Physics,
P.O.Box 162, 1000 Skopje, Republic of Macedonia

The journal computer preparation is done at the Institute of Physics.

Physica Macedonica	**Vol. 62**	**pp. 1 - 47**	**Skopje 2016**

C O N T E N T S

1. B. Radiša, M. Mitrović and B. Misailović **1**
THE EFFECT OF SOLUTION PRE-HISTORYON CHIRALITY OF SODIUM CHLORATE CRYSTALS FROM AQUEOUS SOLUTIONS

2. S. Rendevski, I. Aliu and N. Mahmudi..... **7**
NORMALIZED INTEGRAL FOURIER TRANSFORM AMPLITUDE FOR FOOD QUALITY DETERMINATION BY ACOUSTIC IMPULSE RESPONSE METHOD

3. D. Krstovska and B. Mitreska **13**
NONLINEAR ULTRASOUND WAVE GENERATION IN QUASI-TWO DIMENSIONAL ORGANIC CONDUCTORS

4. O. Atanacković..... **22**
ON TWO EXTREMELY FAST METHODS FOR THE SOLUTION OF THE NON-LTE LINE FORMATION PROBLEM

5. Luljeta Disha, Defrim Bulku and Antoneta Deda..... **34**
METHOD OF ABSOLUTE GRAVITY MEASUREMENT AND ITS INFLUENCE IN MASS DETERMINATION

6. N. Mahmudi and S. Rendevski **41**
GAMMA RADIATION SYNTHESIS OF POLYMERS AND CONTROL OF THE MECHANICHAL PROPERTIES

Институт за физика

Physica Macedonica **62**, (2016) p. 1-6

THE EFFECT OF SOLUTION PRE-HISTORYON CHIRALITY OF SODIUM CHLORATE CRYSTALS FROM AQUEOUS SOLUTIONS

B. Radiša, M. Mitrović and B. Misailović

University of Belgrade-Faculty of Physics, Studentski trg 12, 11000 Belgrade, Serbia

Abstract. The phenomenon of spontaneous chiral symmetry breaking attracts the attention in physics, chemistry and biology. Sodium chlorate crystals are an interesting example of optically active system. In this paper results of investigations of effect of growth history on sodium chlorate crystals chirality will be presented. Crystals were nucleated and grown at T = (28.00±0.02)°C from aqueous solution saturated at T_0 = (31.0±0.1)°C. Prior to nucleation the solution temperature firstly increased to T_{inc}, and then slowly decreased to growth temperature. Obtained results showed that solution pre-history induced the increase in the population of only one of enantiomers, i.e. D-crystals dominated. Results indicate that solution pre-history might affect chiral symmetry breaking in crystallization of sodium chlorate crystals even achieving crystals of chiral purity.

PACS: *81.10.Aj, 81.10.Dn*

1. INTRODUCTION

Chiral symmetry breaking happen when a chemical and physical processes who do not have any priority in production of one or the other of the enantiomer spontaneously give rise to a large number of one of the enantiomers: left-handed (L) or right-handed (D). Considering the energy, there is equal probability for creating and existence both enantiomers. Chiral asymmetry is found everywhere in nature, and one example are living organisms who utilize L-amino acids and D-sugars. The fact that living organisms choose only one type of amino acids and only one type of sugars as a constituent component has intrigued many scientists. Mechanisms which lead to total chiral purity or to transition from one enantiomer to another are of the great interest.

Sodium chlorate ($NaClO_3$) molecules are achiral but they form chiral crystals in the cubic space group $P2_13$.[1] Chiral crystals of sodium chlorate are optically active, and L or D crystals can be easily identified with a pair of polarizers. When polarizers are crossed crystal color changes with rotation of the analyzer (Fig. 1a), i.e. the color of the crystal will be different for clockwise or counterclockwise analyzer rotation depending on the handedness of the crystal (Fig 1b).

Kondepudi et al.[2] showed that stirring during the crystallization of $NaClO_3$ from aqueous solution was sufficient to produce more than 99% of crystals of the same handedness, while in unstirred solution equal number of L and D crystals was obtained. Viedma[3] found that

adding glass flasks and stirring the solution which is consisted of the same number of L and D sodium chlorate crystals, leads to complete deracemization of $NaClO_3$, i.e. one enantiomer disappears completely. Chiral symmetry breaking was also reported in experiments with solution temperature changes (heating and cooling cycles)[4] and for other substances [5,6].

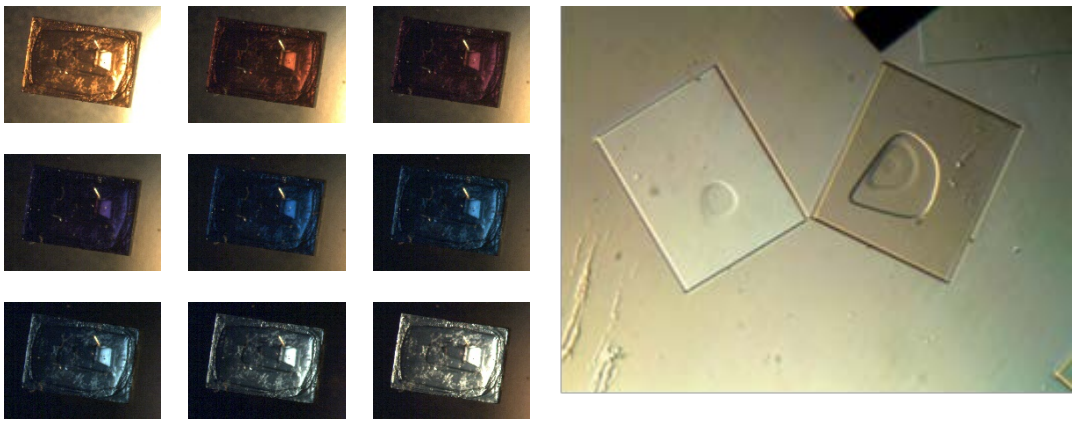

Figure 1. a) Crystal color changes with analyzer rotation b) L and D sodium chlorate crystals in solution.

These results are experimental evidence of chiral symmetry breaking on macroscopic scale induced by autocatalysis and tendency for domination of one enantiomer group. One of explanations of the process of chiral symmetry breaking is secondary nucleation. Namely, it is considered that nucleation of chiral ″mother″ crystal influence the production of generations of secundary nucleated crystals of the same handedness.[7-17] In the paper[18] it was shown that chiral symmetry breaking occurs in primary nucleation, and that secondary nucleation only increase it. Due to that, process of chiral symmetry breaking cannot be explained by the nucleation of ″mother″ crystal, i.e. mechanisms which induce domination of one enantiomer group are still unclear.

In order to explain it, different models were suggested and most of them take in consider first phases of the crystallization. Niinomi et al.[19] showed that in crystallization process driven by evaporation of solvent, achiral metastable crystals of sodium chlorate formed prior to chiral crystals in solution growth, and that transition from achiral to chiral state occurred, which means that the chirality of the $NaClO_3$ crystal emerges during the transition. Differences in solubility of metastable achiral and chiral $NaClO_3$ crystals are also important for describing the phenomenon. [20]

2. EXPERIMENTAL PROCEDURE

All experiments were performed with a saturated solution prepared using the following procedure. An aqueous solution of $NaClO_3$ was prepared by dissolving $NaClO_3$ (Analytical grade of substance was 99% purity) in distilled water at room temperature. Then the solution was heated under stirring with a magnetic hot plate stirrer and then left for a three days at saturation

temperature to precipitate the excess solute and thus to equilibrate the solution. Crystals were nucleated in the cell by introducing air bubbles through a needle into the cell.

We observed in situ crystal growth by digital optical microscope Nikon SMZ800 equipped with a video recording system (camera Luminera, Infinity 1), using a polarized light. Between 15 and 33 crystal nuclei, sufficiently distant to avoid intergrowth during the growth, were preselected for growth rate measurements during each growth run. In order to investigate the influence of solution history on sodium chlorate crystals growth rate and chirality two types of experiments were performed. In all experiments the solution was saturated at temperature $T_0 = (31.0 \pm 0.1)°C$, while the crystal growth was performed at $T_r = (28.0 \pm 0.1)°C$.

Both types of experiments consisted of two parts. In the first part solution temperature was increased to T_{inc}=35.0°C (the first type of experiments) or to T_{inc} = 32.8°C (the second type of experiments), and after that slowly decreased to the growth temperature $T_r = (28.0 \pm 0.1)°C$. The temperature decreasing in the first type of experiments was about 2.5 h, while in the second type was about 4h. Procedure of both types of experiments was similar and the only difference was in initial and the final intervals of temperature change, showed in Table 1. Temperature was changed from T_1 to T_2 in steps of ΔT every 5 min. From 30.8°C to 28.0°C the solution was left to be cooled by itself, in Type 1 experiments, and also for Type 2 experiments in temperature range from 29.6°C to 28.0°C.

Table 1. Temperature changes

Type 1 experiment			Type 2 experiment		
T_1 [°C]	T_2 [°C]	ΔT[°C]	T_1 [°C]	T_2 [°C]	ΔT[°C]
35.0	34.0	0.5	32.8	32.2	0.3
34.0	32.8	0.4	32.2	31.6	0.2
32.8	32.2	0.3	31.6	31.4	0.1
32.2	31.6	0.2	31.4	29.6	0.05
31.6	31.4	0.1	-	-	-
31.4	30.8	0.05	-	-	-

Procedure of the second part of both types of experiments was the same. After the temperature of growth was reached, crystals were nucleated by introducing air bubbles through a needle into the cell. Crystal growth lasted about four hours and in all experiments crystals sizes were measured every 40 minutes.

3. RESULTS AND DISCUSSION

At different experimental conditions growth rate dispersions occurred. Histograms representing these dispersions are presented in Figure 2 and Figure 3. These dispersions are described by simple normal distribution, also included in Figure 2 and 3. Zero growth rates, whose existence is completely unclear,[21] are excluded from fitting procedure. Several high growth rates at the end of dispersions, which probably pertain to higher activity of dominant dislocation group, are excluded from fitting procedure, too.[22]

Number of measured growth rates N, number of measured growth rates of left-handed crystals N_L and number of measured growth rates of right-handed crystals N_D, as well as the most probable growth rate R_1, R_2, R_3 and R_4 for different experiments are presented in Table 2.

It can be seen from Figures 2 and 3, and Table 2 that crystals grown in Type 2 experiments had higher growth rates. This is in accordance with lattice strain theory.[23] Namely, the temperature changes were performed in smaller steps, so crystals had less defects of structure, and consequently higher growth rates.

Table 2. Experimental results

		R_1 [nm/s]	R_2 [nm/s]	R_3 [nm/s]	R_4 [nm/s]
Type 1	N=340	22±4	47.5±0.7	69±2	90±2
	N_L=155	26±4	51.3±0.5		
	N_D=185	21±3	42.8±0.3	65±3	93±4
Type 2	N=160	25±4	51.8±0.7	83±3	
	N_L=18		47.9±0.5		
	N_D=142	25±1	53.0±0.4	82.8±0.8	

Theoretical analysis shows that there is equal probability for creating and existence both enantiomers. Results presented in Table 2 show that in both types of experiments left- and right-handed crystals existed. In Type 1 experiments numbers of L and D crystals are comparable, while in Type 2 experiments right-handed crystals dominated. Due to the fact that in Type 2 experiments the number of L crystals is significantly less than the number of D crystals, conditions might lead to total chiral purity. Also, there was no transition occurred from one enantiomer to another enantiomer.

Regardless this, the influence of crystal growth history is obvious. Further investigations in this field might bring clearer results, and contribute to crystal growth theories development.

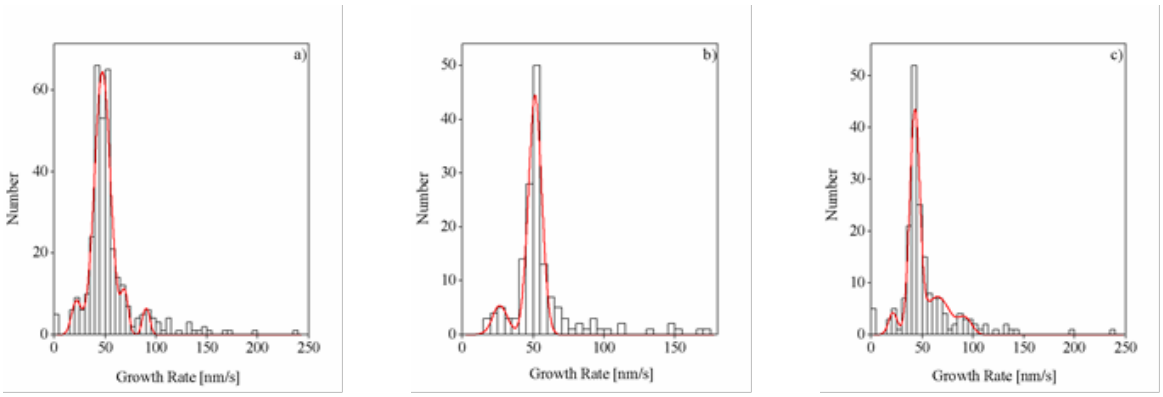

Figure 2. Histograms representing growth rate in direction <100> for Type 1 experiments of: a) all observed crystals b) L crystals c) D crystals.

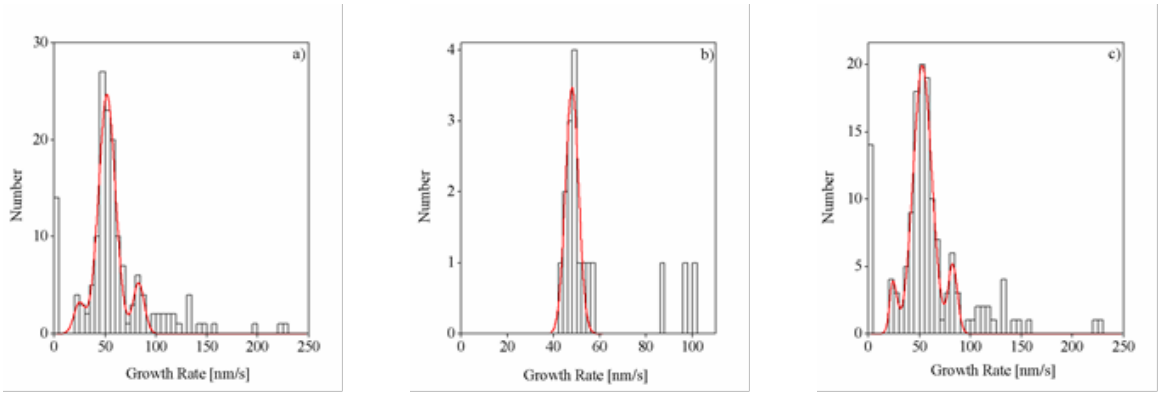

Figure 3. Histograms representing growth rate in direction <100> for Type 2 experiments of: a) all observed crystals b) L crystals c) D crystals.

4. CONCLUSIONS

Mechanisms which lead to total chiral purity are of the great interest. In this paper results of investigations of effect of growth history on sodium chlorate crystals chirality are presented. Two types of experiments were performed. Obtained results show that at different experimental conditions growth rate dispersions is occurred. In experiments Type 2 crystals grown at higher rates. In both types of experiments L and D crystals existed. Solution pre-history induced the increase in the population of D-crystals in experiments Type 2. In experiments performed there was no transition from one enantiomer to another. Obtained results indicate that solution pre-history might affect chiral symmetry breaking in crystallization of sodium chlorate crystals even achieving crystals of chiral purity, which request further investigations.

REFERENCES

[1] W.H.Z.Zacharlasen, Kristallograhie **71**, 517–529 (1929)
[2] D. K. Kondepudi, R. J. Kaufman and N. Singh, Science, **250**, 975–976 (1990)
[3] C. Viedma, Phys. Rev. Lett., **94**, 065504 (2005)
[4] K. Suwannasang, A. E. Flood, C. Rougeot and G. Coquerel, Cryst. Growth Des. **13**, 3498–3504 (2013)
[5] D. G. Blackmond, Proc. Natl. Acad. Sci. U. S. A., **101**, 5732–5736 (2004)
[6] J. E. Hein, B. H. Cao, C. Viedma, R. M. Kellogg and D. G.Blackmond, J. Am. Chem. Soc., **134**, 12629–12636 (2012)
[7] J. M. McBride, R. L. Carter, Angew. Chem., Int. Ed. Engl. **30**, 293−295 (1991)
[8] D. K. Kondepudi, K. L. Bullock, J. A. Digits, J. K. Hall, J. M. Miller, J. Am. Chem. Soc. **115**, 10211−10216 (1993)
[9] R. Y. Qian, G. D. Botsaris, Chem. Eng. Sci. **52**, 3429−3440 (1997)
[10] R. Y. Qian, G. D. Botsaris, Chem. Eng. Sci. **53**, 1745−1756 (1998)

[11] T. Buhse, D. Durand, D. Kondepudi, J. Laudadio, S. Spilker, Phys. Rev. Lett. **84**, 4405−4408 (2000)
[12] R. Y. Qian, G. D. Botsaris, Chem. Eng. Sci. **59**, 2841−2852 (2004)
[13] D. K. Kondepudi, C. Sabanayagam, Chem. Phys. Lett. **217**, 364−368 (1994)
[14] B. Martin, A. Tharrington, X.-I. Wu, Phys. Rev. Lett. **77**, 2826−2829 (1996)
[15] J. H. E. Cartwright, J. M. García-Ruiz, O. Piro, C. I. S. Díaz, Tuval, Phys. Rev. Lett. **93**, 035502 (2004)
[16] J. H. E. Cartwright, O. Piro, Tuval, I. Phys. Rev. Lett. **98**, 165501 (2007)
[17] M. Uwaha, J. Phys. Soc. Jpn. **73**, 2601−2603 (2004)
[18] C. Viedma, J. Cryst. Growth **261**, 118−121 (2004)
[19] H. Niinomi, T. Yamazaki, S. Harada, T. Ujihara, H. Miura,Y. Kimura, T. Kuribayashi, M. Uwaha, and K. Tsukamoto, Cryst. Growth Des. **13**, 5188−5192 (2013)
[20] H. Niinomi, A. Horio, S. Harada, T. Ujihara, H. Miura, Y. Kimura, K. Tsukamoto, J. Cryst. Growth **394**, 106–111 (2014)
[21] B. M. Misailović, D. A. Malivuk, A. A. Žekić, M. M. Mitrović, Cryst. Growth Des. **14**, 972-978 (2014)
[22] M. M. Mitrović, A. A. Žekić, B. M. Misailović, B. Z. Radiša, Ind. Eng. Chem. Res. **53 (50)**, 19643-19648 (2014)
[23] A. E. D. M. van der Heijden, J. P. van der Eerden, J. Cryst. Growth **118**, 14-26 (1992)

Институт за физика

Physica Macedonica **62**, (2016) p. 7-12

NORMALIZED INTEGRAL FOURIER TRANSFORM AMPLITUDE FOR FOOD QUALITY DETERMINATION BY ACOUSTIC IMPULSE RESPONSE METHOD

S. Rendevski[1*], I. Aliu[2] and N. Mahmudi[2]

[1]*Faculty of Engineering and Technology, Department of Mathematics and Physics, Higher Colleges of Technology, Ras al Khaimah Men's Campus, United Arab Emirates*

[2] *Faculty of Natural Sciences and Mathematics, State University of Tetovo, bul. Ilinden, b.b., 1200 Tetovo, Republic of Macedonia*

Abstract. The research has been conducted with the goal of determining the shelf-life of post harvested tomatoes by implementing the non-destructive physical method of acoustic impulse response. Normalized integral Fourier transform amplitude has been introduced for enhancing the precision of shelf-life determination in comparison to the use of the well-known firmness parameter F_i. The firmness coefficient F_i has been calculated on the basis of the dominant (fundamental) frequency of tomato response signal f and sample mass m. The Fast-Fourier transform algorithm has been used on the acoustical time dependent electrical signals taken from an acoustical sensor attached to the product under investigation, thus allowing the frequency dependent Fourier transform to be found.

PACS: 43.40.+s, 45.10.-b, 46.40.-f, 87.19.r-

1. INTRODUCTION

For assessing the quality of agricultural products beyond the use of chemical and biochemical methods, great practical importance has been given recently to the physical methods, especially the non-destructive methods that are fast, accurate and reliable [1.2]. One such method is the acoustic impulse response method, which has been investigated by many researchers aiming at measuring the firmness of fruits and vegetables [3-5]. The method gives solid results that were proven by the classical destructive firm testing technique [6]. The main advantage of the acoustic impulse response method is that it is fast, reliable, non-destructive and can be performed in-field (on-site). The main disadvantage of the method is that it gives a "bulk" information for the product, which means the acoustic response is like averaged for the whole sample. Only the magnetic resonance imaging method (MRI) can give perfect picture of the inside structure of the food product examined, but this method requires expensive equipment and highly trained examiner [7]. The major achievement of the acoustic impulse response method is seen in the context of good correlation of the results for maturity stage of food samples with the results from

many other methods [8]. That means that the acoustic impulse response method can be used by alone.

2. MATERIALS AND METHODS

The "Melody" variety tomatoes (*Lycopersicum*) were hand-harvested from the greenhouse orangery of the company "Agroproduct" from Gostivar, Republic of Macedonia, on October 17, 2013. Twenty seven tomatoes were sorted according to their mass (250 g ± 50 g) and color appearance of same class (90% of the surface to be red and 10% of the surface showing change from green to yellow). For that purpose, a color sensor panel have been composed of five assessors experienced in tomato assessment. Tomatoes were harvested from the tomato trees between 40 – 45 cm above the ground. Only one tomato was taken from a tomato tree. The tomatoes were grown according to the following conditions: average temperature of 14 – 16 ^{0}C during nights; water supply of 1.5 L for 24 hours; fertilizer "Jara" of 180 g per tomato tree; pesticides treatment every week; insecticides treatment on occasions. Tomatoes were stored at 15 ± 1 ^{0}C, relative humidity 60% and were placed in a box that can hold each tomato separated. After been harvested, tomatoes were transferred to the lab and kept during the investigation on average temperature of 15 ± 1 ^{0}C and relative humidity 60 % on shelves with artificial illumination same as under selling condition on the local market.

According to the acoustic impulse response method, tomatoes were impacted without a damage with a small ball pendulum and tomatoes vibration response signals were recorded with a microphone as a sensor. The firmness coefficient F_i has been calculated on the basis of the dominant (fundamental) frequency of tomato response signal f and sample mass m. The firmness coefficient F_i, which for spherical-like fruits was first proposed by Abbott [9] and was modified by Cooke and Rand [10], has been calculated according to the following formula:

$$F_i = f^2 m^{\frac{2}{3}}. \tag{1}$$

Same method has been applied from many researchers on various products (apples, watermelons, mangos, and many others) [11, 12]. To reduce errors due to sample internal homogeneity differences as well as injuries after the collision with the impactor (pendulum ball), it is preferred to change the position of impact and the average response is obtained after three hits on the equatorial surface of the samples when the microphone is positioned at angle 120^0 in respect to the impact [10].

The dominant or fundamental frequency of vibration of the food product has been determined by doing Fourier transform of the amplitude-time function of the sensor signal which gave the amplitude-frequency function (so called power spectrum). There are several methods described in the literature for calculating the Fourier transform and we used the Fast Fourier Transform algorithm incorporated in the powerful OriginPro® graphical analysis software. This software combines some good features from MatLab® and Mathematica®.

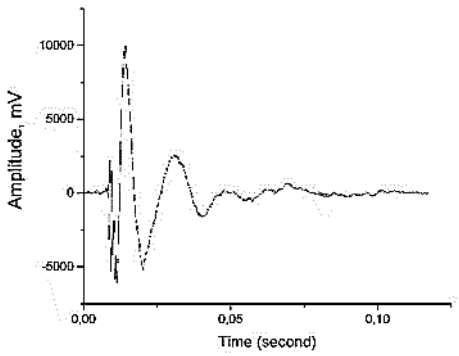

Figure 1. Typical acoustic signal.

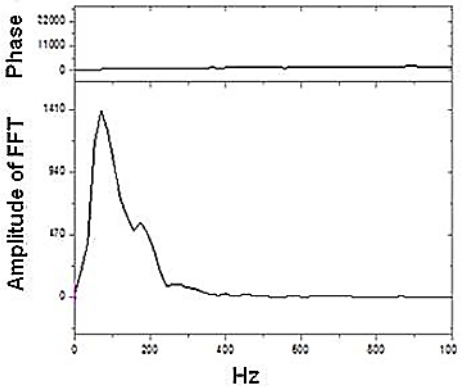

Figure 2. Fourier transform of the signal from fig.1

On figure 1, a common acoustical sensor signal is given after impact on a tomato, and on figure 2, the Fourier transform is given for the same function. It is obvious that the dominant frequency *f* of the sample vibration has a value of 95 Hz, but there is also another small peak in the function at 180 Hz and on some cases there were more. The position of the main, or the dominant frequency, and the presence of other peaks in the Fourier transform can give more information about the food product. For example, if there is second smaller peak, that means the vibration of the sample is more complex, probably because of different internal structure inside the product – already rotten regions, over-ripen small regions that will spread in the following days, large inside inhomogeneity in density of the product because of changes in grown conditions, and so on. When focused only of the main peak or the dominant frequency of vibration, the shift over time to lower values indicates softer product and/or separations inside of the product – one larger region with more water content and another (a core) denser (less water content) which is typical for over-mature stage of fruits and vegetables.

Some detailed information from the acoustic impulse response method as well as the use of piezoelectric or microphone as a sensor applied for tomato quality assessment after storage has been given in literature [2-5]. In our research, we used equipment schematically described on figure 3. Here, we have a ring sample holder that gently hold the tomato sample; impactor with a pendulum ball (self-made with aluminum ball of 20 g mass and pendulum angle 30^0 that catch the ball back after the first impact); microphone model MI-10, A4 Tech, Taiwan, with integrated amplifier and a computer for data acquistion and calculations. GoldWave® audio studio software has been used for taking the amplitude-time signal from the microphone. The sampling rate was 20,000 points per second.

In this paper, a new quantity determined from the Fourier transform of the acoustical signal, named normalized integral amplitude, *N*ia, has been introduced (in units of Hz). The normalized integral amplitude is obtained after integration of the Fourior transform function on the whole frequency range and by division after by the amplitude at the dominant frequency.

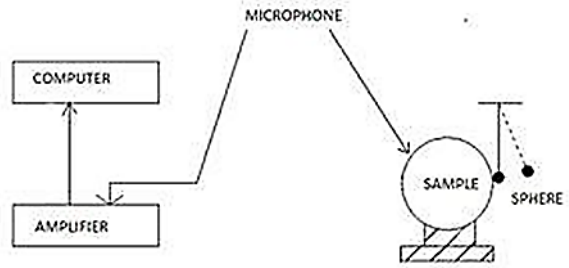

Figure 3. Scheme of the equipment for acoustic impulse response measurements.

From the physics of sound and mathemaics of the Fourier transform it is known that according to the Parseval's theorem the energy of the acoustical signal received by the microphone $\int_{-\infty}^{+\infty} |f(t)|^2 dt$ is equal to the energy of the vibrational spectrum of the sample obtained from the Fourier transform $\int_{-\infty}^{+\infty} |F(\omega)|^2 d\omega$ [13, 14]. Knowing this, it is obvious that *N*ia is directly proportional to the energy of the signal (or the vibrational spectrum) and after normalizing it to the maximum amplitude, *N*ia can be considered as a parameter that gives information on the "dissipation" of the energy not only around the dominant frequency of vibration, but on the whole spectrum, indeed.

In the literature, when acusto-vibrational properties are expressed with only the dominant frequency, the contribution to all other frequencies of vibration in the obtained Fourier transform function is taken as negligible. The aim here is not to connect *N*ia quantity to the firmness properties of samples, as Abbott (1968) and Cooke and Rand (1973) did, but to check the behavior of the quantity over storage time passed.

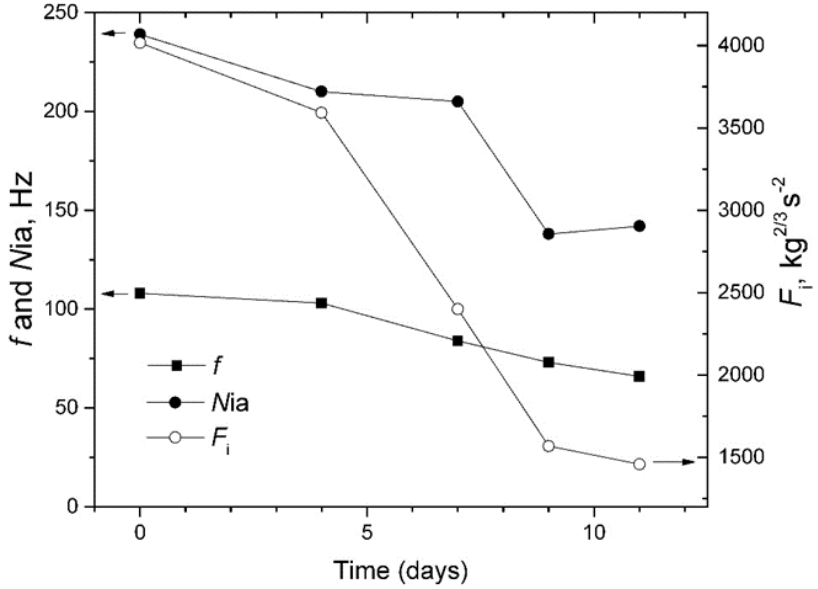

Figure 4. Graphical presentation of the changes of *f*, *N*ia and F_i over time.

It is expectable to have drastic change of *N*ia value if several more vibration characteristics exist (peaks) beside the dominant one in the sample. Aiming to understand the importance of *N*ia quantity, the Fourier transform function for over-matured sample will be discussed in comparison to same sample for which the Fourier transform function has been taken immediately after harvesting. The values of *N*ia parameters were 168 Hz and 202 Hz, respectively, while the values of the dominant frequency where 73 Hz and 102 Hz, respectively. In the research presented it has been found that when the difference between the *N*ia value and *f* is more than double, the product can be considered as over-matured, as in the above example when we found *f* = 73 Hz and *N*ia = 168 Hz. When time dependences of *N*ia and *f* is constructed, there is more drastic change of *N*ia value than *f* value after some critical moment (fig.4). This moment is direct indication of the shelf-life of the tomatoes because after this critical time the quality of the sample deteriorates significantly.

3. RESULTS, DISSCUSIONS AND CONCLUSIONS

The mass of the tomatoes are important quantities for determination of the firmness parameter, according to Eq.1. The mass was measured each experimental day using the electronic weighing scale with precision of 1 g. Mass loss was calculated according to the equation $m_l = [(m_i - m_f) / m_i] \cdot 100\%$, where m_l is the reduced mass in percentage, m_i is the initial mass and m_f is the final mass of the product, in grams. It has been found during the research that the reduced mass was about 5% of the initial mass of all tomatoes. This is due to the water loss during the 11 days period of investigation. However, such a loss of mass was not considered influential on the change in maturity stage of the product in investigated period.

The values of the dominant (fundamental) frequency of vibration *f*, normalized integral amplitude *N*ia, firmness parameter F_i calculated from Eq.1, are given in Table 1.

Table 1. Main parameters obtained from the acoustic impulse response method.

Time (in days)	*f*,Hz	*N*ia,Hz	F_i, $kg^{2/3}/s^2$
0	108 ± 11	239 ± 18	4017
4	103 ± 10	210 ± 20	3592
7	84 ± 15	205 ± 22	2400
9	73 ± 17	138 ± 20	1568
11	66 ± 12	142 ± 23	1458

From fig.4, it is obvious that the change of *N*ia over time are more pronounced in comparison to the changes of *f*. The change of *N*ia is following an inverse S graphical dependence from which it is visible that after 9 days of storage there is significant decrease of *N*ia value which indicates over-mature stage of the tomatoes. The same behavior has been found when changes of the firmness parameter F_i have been followed over days passed (fig.4). This indicates that *N*ia quantity can be considered as a measure for the vibration characteristics of the tomato, instead of the single dominant frequency of vibration. The dependence of *N*ia over time is following the dependence of F_i in more profound way than the *f*. That implies that there is direct connection between *N*ia and F_i that requires theoretical investigation henceforth.

As seen from the results from the application of the acoustic impulse response methods, for the "Melody" type tomatoes kept at 15 ^{0}C at 60 % relative humidity and normal illumination, the shelf-life has been found for nine days of storage.

The method of acoustic impulse response provides a "view" of the internal homogeneity of tomatoes without destructing them and for this reason it is considered as a method of non-destructive testing of products. If there is inhomogeneity inside tomatoes, that will be reflected through different dominant frequencies and normalized integral amplitude of the product vibrations during slight impact of the tomatoes in different positions, for example, around the stem, at the bottom of the fruit or in the equatorial part.

REFERENCES

[1] Gunasekaran, S. "Nondestructive food evaluation: Techniques to analyze properties and quality". New York, USA: CRC Press (2000)
[2] Kilcast, D. "Instrumental assessment of food sensory quality: A practical guide". Cambridge, UK: Woodhead Publishing (2013)
[3] Galili, N., Shmulevich, I., Benichou, N. Transactions of the American Society of Agricultural Engineering, **41**, 399-407 (1998)
[4] Duprat, F., Grotte, M., Pietri, E., Loonis, D., Studman, C.J. Journal of Agricultural Engineering Research, **66(4)**, 251-259 (1997)
[5] Aboonajmi, M., Jahangiri, M., Hassan-Beygi, S.R. Journal of Food Processing and Preservation, **39(6)**, 3175-3188 (2015)
[6] Barrett, D.M., Beaulieu, J.C., Shewfelt, R. Critical Reviews in Food Science and Nutrition, **50(5)**, 369-389 (2010)
[7] Zhang, L., McCarthy, M.J. Postharvest Biology and Technology, **67**, 37-43 (2012)
[8] Arana, I. "Physical properties of food". Boca Raton, USA: Taylor & Francis Group (2012)
[9] Abbott, J.A., Bachan, A., Childers, G.S., Fizterald, J. V., Matusik, F. J. Food Technology, **22**, 635-645 (1968)
[10] Cooke, J. R., Rand, R. H. Journal of Agricultural Engineering Research, **18**, 141-157 (1973)
[11] Abbott, J.A. Quality of Fresh and Processed Fruits, **542**, 265-279 (2004)
[12] Butz, P., Hofmann, C., Tauscher, B. *Journal of Food Science*, **70(9)**, 131-141 (2005)
[13] Pain, J.H. "The physics of vibration and waves". Chichester, UK: John Wiley and Sons (2005)
[14] Urumov, V. "Mathematical physics: methods, applications and problems (in Macedonian)". Skopje, Republic of Macedonia: Prosvetno Delo (1997)

Институт за физика

Physica Macedonica **62**, (2016) p. 13-21

NONLINEAR ULTRASOUND WAVE GENERATION IN QUASI-TWO DIMENSIONAL ORGANIC CONDUCTORS

D. Krstovska and B. Mitreska

Institute of Physics, Faculty of Natural Sciences and Mathematics, Ss. Cyril and Methodius University, P. O. Box 162, 1000 Skopje, Macedonia

Abstract. The amplitude of an ultrasound wave with double frequency 2ω generated by Joule heating as a heat source in the quasi-two dimensional layered organic conductor β−(BEDT-TTF)$_2$IBr$_2$ is analyzed as a function of the magnetic field strength and its orientation with respect to the plane of the layers. Angular oscillations of the ultrasound wave amplitude are correlated with the changes of electrical and thermal conductivity of the compound when the magnetic field is tilted from the normal to the layers plane due to the periodic dependence of the carriers velocity along the less conducting axis on the field orientation. The period of oscillations allows the characteristic parameters of the Fermi surface to be determined. The magnetic field dependence reveals that the effect of nonlinear generation of the ultrasound wave due to Joule heating is quadratic in proportion to the magnetic field at each field direction. The behavior of the wave amplitude is different depending on the field orientation from the normal to the layers, i.e., is it oriented at the maximum or minimum in the angular dependence. In layered organic conductors due to the small electron mean free-path the nonlinear generation of ultrasound waves can be observed for a wide range of magnetic fields providing possibilities for experimental studies using non-contact ultrasonic techniques.

PACS: *74.70.Kn, 72.15.Jf, 72.50.+b*

1. INTRODUCTION

The mechanisms of linear transformation, which are responsible for the generation of ultrasound in conducting media at the frequency of an electromagnetic wave ω incident on the surface of the metal, are a standard subject of investigation in electromagnetic-acoustic conversion problems [1-6]. In conducting media, the mechanism occurs as follows: when an electromagnetic wave with frequency ω is incident on the conductor, nonuniform temperature oscillations of the same frequency appear as a result of the thermoelectric effect. These oscillations, in turn, generate acoustic oscillations in the conductor with a frequency that coincides with the frequency of the incident electromagnetic wave (contactless excitation of ultrasound).

The induction [7-10] and deformation force [11-18] have been studied in greatest detail as sources of linear transformation of waves. In the last few years the focus of investigations of electromagnetic excitation of ultrasound has shifted to the study of subtle nonlinear conversion mechanisms. Some studies in ordinary metals have shown that these mechanisms could also generate ultrasound wave with frequency 2ω, i.e., in the nonlinear regime [19-23].

Apart from the induction and deformation forces, longitudinal ultrasound at double frequency can also be generated by other source of nonlinearity. The most important such source is the force arising due to the appearance of thermoelastic stresses in the Joule-heated skin layer [24]. Joule heating is the characteristic of material that can be heated up when there is current flow because electrical energy is transformed into thermal energy. The thermoelectric mechanism of ultrasound generation is in principle a nonlinear interaction due to the action of the thermoelastic stresses on the crystal lattice. These stresses that are caused by the temperature oscillations with frequency 2ω ($\Theta \sim \cos(2\omega t)$) arising from the alternating part of the Joule heat generate ultrasonic waves with double frequency.

In this paper we study the effect of Joule heating from electric currents flowing through a quasi-two dimensional organic conductor on the temperature distribution and nonlinear generation of a longitudinal ultrasound within the conductor. The quasi-two dimensional (q2D) charge-transfer salts form the largest organic superconductor family with unusual normal and superconducting properties which come out of the layered structure as well as the specific shape of the Fermi surface. Their most remarkable feature is the reduced dimensionality of the electronic band structure caused by the specific character of their crystal structure. Specifically, the q2D organic conductor β–$(BEDT\text{-}TTF)_2IBr_2$ is considered and the amplitude of the generated longitudinal ultrasound is analyzed as a function of the magnetic field strength and its orientation from the less conducting axis to the plane of the layers.

2. FORMULATION OF THE PROBLEM

The ultrasound with double frequency is generated as a result of temperature oscillations which are induced by Joule heating as a heat source. Here we consider a case when electric currents flowing through the conductor are along the most conducting axis (x-axis), $\mathbf{j} = (j_x, 0, 0)$ and the only nonzero component of the electric field is the x–component, $\mathbf{E} = (E_x, 0, 0)$. An ultrasound of double frequency is generated and propagating along the less conducting axis (z-axis), $\mathbf{k} = (0, 0, k)$, and therefore all of the quantities depend only on the z–component. The conductor is placed in magnetic field oriented at an angle θ from the normal to layers plane, in the yz plane, $\mathbf{B} = (0, B\sin\theta, B\cos\theta)$. A temperature oscillating with frequency 2ω can occur if $2\omega\tau << 1$ where τ is the relaxation time of the conduction electrons. We study the case of normal skin effect when the condition $k_T l << 1$, where l is the electron mean-free path length and k_T is the thermal wave number, is satisfied.

The complete system of partial differential equations, describing the generation of longitudinal ultrasound at frequency 2ω, includes Maxwell's equations for the magnetic **B** and electric **E** field, the kinetic equation for the nonequilibrium correction χ to the electron distribution function, and the equations of heat conduction and elasticity:

$$\begin{aligned} &\operatorname{curl}\mathbf{B} = \mu_0\mathbf{j}; \quad \operatorname{curl}\mathbf{E} = -\frac{\partial\mathbf{B}}{\partial t}, \quad \left(\frac{\partial}{\partial t} + \mathbf{v}\nabla + e\left[\mathbf{vB}\right]\frac{\partial}{\partial\mathbf{p}} + \frac{1}{\tau}\right)\chi = -e\mathbf{vE}, \\ &-2i\omega C - \kappa_{zz}\frac{\partial^2\Theta}{\partial z^2} = Q_J, \quad \frac{\partial^2 U_{2\omega}}{\partial z^2} + k_s^2 U_{2\omega} = \beta\frac{\partial\Theta}{\partial z}. \end{aligned} \tag{1}$$

Here **v** and **p** are the electron velocity and momentum, e is the electron charge, Θ is the high-frequency addition to the mean temperature T of the crystal, Q_J is the power density of the heat source, C is the volumetric heat capacity, κ_{zz} is the thermal conductivity tensor, $k_s = 2\omega/s$ is the wave vector of the ultrasonic wave at frequency 2ω, s is the ultrasound wave velocity and β is the volumetric expansion coefficient.

The above system of equations must be supplemented with the corresponding boundary conditions for the heat flux and the ultrasound amplitude at the conductor's surface. In the case when the heat source is the time-dependent part of the Joule heating the boundary conditions are:

$$\kappa_{zz}\frac{\partial\Theta}{\partial z}|_{z=0}=0, \qquad \frac{\partial U_{2\omega}}{\partial z}|_{z=0}=-\beta\frac{\partial\Theta}{\partial z}|_{z=0}. \tag{2}$$

By using Maxwell's equations one obtains the following expression for the Joule heating

$$Q_J=\mathbf{jE}=j_xE_x=\frac{i\omega B_y^2}{\mu_0}e^{2i(kz-\omega t)}, \tag{3}$$

where $k=(1+i)/\delta$ and $\delta=\sqrt{2/(\omega\mu_0\sigma_{xx})}$.

Substituting eq. (3) into the heat conduction equation (third equation in (1)) we obtain the following expression for the temperature distribution

$$\frac{\partial^2\Theta}{\partial z^2}+k_T^2\Theta=\frac{i\omega B_y^2}{\kappa_{zz}\mu_0}e^{2i(kz-\omega t)}, \tag{4}$$

where $k_T=(1+i)/\delta_T$ and $\delta_T=\sqrt{\kappa_{zz}/\omega C}$. Here δ_T is the penetration depth of the thermal field under the conditions of a normal skin effect.

The solution of eq. (4) is given as

$$\Theta(z)=\frac{i\omega B^2\sin^2\theta}{\kappa_{zz}\mu_0}\frac{e^{2ikz}-\frac{2k}{k_T}e^{ik_Tz}}{k_T^2-4k^2}. \tag{5}$$

The complex amplitude of the generated longitudinal ultrasound wave with double frequency can be written in the following form

$$U_{2\omega}=2i\beta\frac{B^2\sin^2\theta}{\mu_0qC}\frac{\delta}{\delta+2\delta_T} \tag{6}$$

The components of the conductivity tensor which relate the current density to the electric field can be calculated by using the Boltzmann transport equation for the charge carrier distribution function, based on the tight binding approximation band structure within the single relaxation time approximation τ (second equation in (1)) [25]. The components of the electrical conductivity tensor are determined as follows

$$\sigma_{ij} = \frac{2e^3 B}{(2\pi\hbar)^3} \int \frac{\partial f_0}{\partial \varepsilon} d\varepsilon \int dp_B \int_0^T dt v_i(t) \chi_j . \tag{7}$$

Here $\hbar$ is the Planck's constant divided by 2π, $p_B = p_y \sin\theta + p_z \cos\theta$ =const is the momentum projection in the magnetic field direction, and t is the time motion of the conduction electrons in the magnetic field under the influence of the Lorentz force d**p**/dt =e (**v**×**B**).

For the quasi-two dimensional organic conductor whose electron energy spectrum has the form

$$\varepsilon(p) = \frac{p_x^2 + p_y^2}{2m^*} + \eta \frac{v_F \hbar}{c} \cos\left(\frac{c p_z}{\hbar}\right), \tag{8}$$

where m^* is the electron cyclotron effective mass, η is the quasi-two dimensionality parameter, v_F is the characteristic Fermi velocity of the electrons along the layers, c is the lattice constant, the expressions for σ_{zz} and σ_{xx} take the following form

$$\sigma_{zz} = \sigma_0 \cos\theta J_0^2\left(\frac{cD_p \tan\theta}{\hbar}\right) \quad \text{and} \quad \sigma_{xx} = \frac{h^2}{B^2 \cos^2\theta}(\sigma_0 + \sigma_{zz} \tan^2\theta). \tag{9}$$

Here σ_0 coincides in order of magnitude with the electrical conductivity along the layers in the absence of a magnetic field, $Dp = 2p_F$ is the averaged diameter of the Fermi surface along the p_y axis and $h = e/m* \tau$.

The thermal conductivity κ_{zz} is obtained by using the Wiedemann-Franz law

$$\kappa_{zz} = \frac{\pi^2 k_B^2 T}{3e^2} \sigma_{zz}, \tag{10}$$

where k_B is the Boltzmann constant.

3. RESULTS AND DISCUSSION

The amplitude of the generated ultrasound wave with double frequency due to Joule heating is a function of the frequency of applied electric current ω, the magnetic field B, the angle between the normal to the layers and the magnetic field θ, as well as of the characteristics of the q2D conductor (electrical and thermal conductivity). For the q2D organic conductor β–(BEDT-TTF)$_2$IBr$_2$, the interlayer transfer integral and the cyclotron mass extracted from data on magnetic quantum oscillations are t_c = 0.35 meV and $m^* = 4.2m_e$, respectively and the relaxation time is of the order of 10 ps [26]. The Fermi surface is a weakly warped cylinder and the quasi-two dimensionality parameter is of order $\eta = 10^{-3}$.

Figure 1 shows the angular dependence of the amplitude $U_{2\omega}(\theta)$ for several field values with pronounced peaks at certain angles whose height decreases with increasing angle between the normal and the plane of the layers. There is a deep minimum for the orientation of the magnetic field in the plane of the layers. The angular oscillations are characteristic of the kinetic and

thermoelectric coefficients of layered organic conductors. The oscillatory dependence of the ultrasound wave amplitude $U_{2\omega}$ on the angle θ is determined by the angular oscillations of the magnetoresistance $\rho_{zz} = \sigma_{zz}^{-1}$ as well as thermal conductivity κ_{zz} which are associated with the charge carriers motion on the cylindrical Fermi surface in a tilted magnetic field.

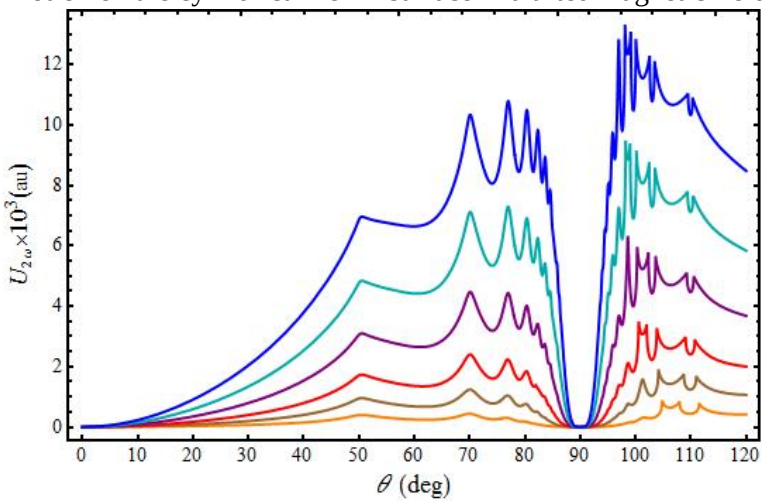

Figure. 1: Angular dependence of the ultrasound wave amplitude $U_{2\omega}$ for T = 30 K, $\eta = 10^{-3}$ and several field values B = 3, 4.5, 6, 8, 10 and 12 T from bottom to top.

In the vicinity of angles where the amplitude $U_{2\omega}$ has maximum value, $\theta_n = \theta_n^{\max}$, the average drift velocity $\bar{v}_z$ of charge carriers along the ultrasound wave vector coincides with the velocity *s* of the ultrasound wave, and their interaction with the wave is most effective. As a result, at these angles the amplitude is the largest (especially this trend is apparent for $\theta > 45^{\circ}$) and $U_{2\omega}$ (θ) exhibits peaks in the angular dependence. The magnitude of the peaks is modulated with changing the tilt angle θ due to the oscillating zeroth order Bessel function $J_0(cD_p \tan\theta/\hbar)$.

If the vectors $\mathbf{k}_S$ and **B** are not orthogonal, the average velocity of charge carriers in the direction of propagation of the wave differs from zero for any shape of the Fermi surface, i.e., charge carriers drift in the direction of wave propagation. The existence of points at which the interaction with the wave is most effective on different trajectories leads to a resonant dependence of the acoustic wave amplitude on magnetic field **B** and the angle between the normal to the layers and magnetic field θ. At $\theta < \pi/2$ the charge carriers which are in phase with the acoustic wave propagating along the *z*−axis are the carriers with time-averaged drift velocity $\bar{v}_z = \eta v_F$ in the direction of propagation of the ultrasound wave.

The interaction of these electrons with the ultrasound wave is most effective when $k_s\delta_T << 1$ under the condition of normal skin effect, $k_T l << 1$, and when the q2D closed orbits are not strongly warped. For $\theta < \pi/2$ all orbits of electrons whose states belong to the corrugated cylinder are closed and do not contain self-intersections. Cross-sections of the corrugated cylinder with the plane p_B = const become more elongated with tilting the field away from the *z*−axis. For θ close to $\pi/2$ there is a significant transformation of the electron trajectories in the momentum space. Due to the pronounced elongation of the closed orbits the amplitude of the ultrasound wave $U_{2\omega}$ rapidly decreases with increasing angle as seen in Fig. 1.

For the amplitude $U_{2\omega}$ plotted versus $\tan\theta$ (Fig. 2), the same trends are apparent, but important feature to emphasize is that the amplitude $U_{2\omega}$ is nonzero in the whole range of angles in comparison to the amplitude of the fundamental wave U_{ω} generated by the thermoelectric forces in the linear electromagnetic-acoustic transformation processes in q2D organic conductors [27]. This is because of the $\sin\theta$ factor in the denominator of the expression for the amplitude $U_{2\omega}$ (eq. 6).

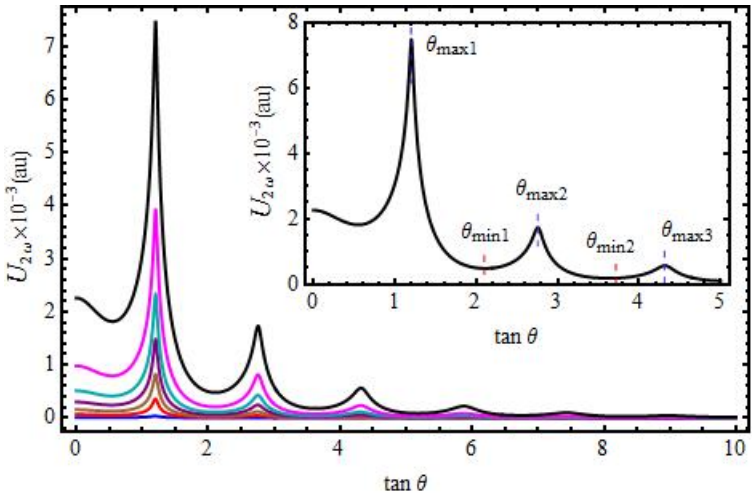

Figure. 2: tan θ dependence of the ultrasound wave amplitude $U_{2\omega}$ for T = 30 K, $\eta = 10^{-3}$ and several field values B = 3, 6, 8, 10, 12, 15 and 20 T from bottom to top. The inset shows the tan θ dependence of the amplitude $U_{2\omega}$ for T = 30 K, $\eta = 10^{-3}$ and B = 20 T with the corresponding Yamaji angles where the amplitude $U_{2\omega}$ has maximum or minimum value.

When $cD_p \tan\theta/\hbar$ equals a zero of the zeroth-order Bessel function, then at that angle the electrical conductivity along the less conducting axis, $\sigma_{zz}(\theta)$, will be negligible and the magneto-resistance $\rho_{zz}(\theta)$ will be a maximum. These angles are known as Yamaji angles [28, 29]. If $cD_p \tan\theta/\hbar >> 1$, then the zeros occurs at angles $\theta_n = \theta_n^{\max}$, given by $cD_p \tan\theta_n^{\max}/\hbar = \pi(n - 1/4)$, n = 0, 1, 2, 3, … For $\rho_{zz}(\theta)$ to be a minimum it should be $\theta_n = \theta_n^{\min}$, where $cD_p \tan\theta_n^{\min}/\hbar = \pi(n + 1/4)$. According to eqs. (6) and (9), the amplitude $U_{2\omega}$ has a peak or dip at angles where $\rho_{zz}(\theta)$ is maximum or minimum as expected in case when there exist only closed Fermi surface sections. This is plotted in the inset of Fig. 2 for B = 20 T where the corresponding angles are marked at which the amplitude $U_{2\omega}$ has a peak or dip, respectively. Also, the tan θ position of the peaks and dips is field independent, i.e., does not change with increasing field. The narrow peaks that appear in the $U_{2\omega}$ (tan θ) dependence repeat with a period $\Delta(\tan\theta) = 2\pi\hbar/cD_p$. The experimental measurements of the period will allow the diameter D_p of the Fermi surface to be determined. In addition, from the shift between the tan θ positions where $U_{2\omega}$ (tan θ) is minimum and tan θ positions where $U_{2\omega}$ (tan θ) has a peak the value of the interlayer transfer integrals t_c in the energy dispersion could be calculated.

Next we look at the curves of the amplitude $U_{2\omega}$ as a function of magnetic field at fixed angles. Particularly, the angles where $U_{2\omega}(\theta)$ has maximum and minimum value, determined from the inset of Fig. 2, will be considered. Figure 3 shows the traces of $U_{2\omega}$ (B) for several field

directions from the normal to the layers: θ = 3°, 10°, 15°, 28°, 50.05°, 64.78°, 75°, 83° and 90°. The effect of generation of the ultrasound wave due to Joule heating is quadratic in proportion to the magnetic field at each field direction. It is important to note that the field behavior of the ultrasound wave amplitude $U_{2\omega}$ is quite distinct for $\theta_n = \theta_n^{\max}$ and $\theta_n = \theta_n^{\min}$. While for angles where the amplitude $U_{2\omega}$ has a peak in the angular dependence, for example at the firs peak $\theta_1^{\max} = 50.05^\circ$ in Fig. 3, it is increasing with increasing field without any changes, for angles where the amplitude $U_{2\omega}$ has a dip, as for $\theta_1^{\min} = 64.78^\circ$, there is a narrow peak in the magnetic field dependence at lower fields (inset of Fig. 3). This peak is also present for small angles from the *z*-axis but with smaller amplitude compared to that for $\theta_n = \theta_n^{\min}$ as shown in the inset of Fig. 3.

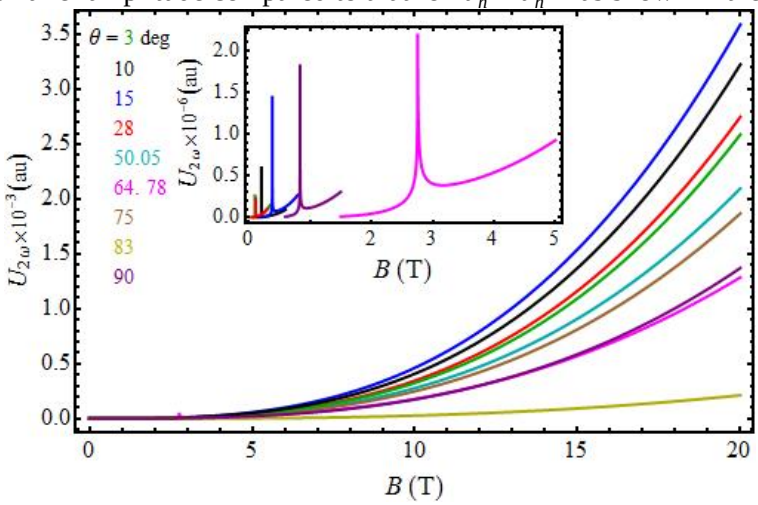

Figure. 3: Magnetic field dependence of the ultrasound wave amplitude $U_{2\omega}$ for T = 30 K and several field directions from the normal to the layers: θ = 3°, 10°, 15°, 28°, 50.05°, 64.78°, 75°, 83° and 90°. The inset shows the low field behavior of $U_{2\omega}$ for T = 20 K, $\eta = 10^{-3}$ and θ = 3°, 10°, 15°, 28°, 64.78° and 90°.

This implies that at angles where the amplitude $U_{2\omega}$ is small, below $\theta = 45^\circ$ (tan θ < 1) and at $\theta_n = \theta_n^{\min}$, compared to its magnitude at the peaks there is always a narrow peak in the field dependence. The appearance of the peak could be associated with a resonant condition in the dependence of the ultrasound wave amplitude on magnetic field B due to the large local temperature gradient induced by the Joule heating at lower fields. The position of the peak and the fulfillment of the resonant condition are field and angle dependent.

The observation of nonlinear ultrasound wave generation due to Joule heating as a heat source is constraint by the condition $2\omega\tau << 1$. In the organic conductor β–(BEDT-TTF)$_2$IBr$_2$ this condition is always fulfilled, even at high frequencies $\omega = 10^8$-10^9 Hz, as the relaxation time τ is very small (for β–(BEDT-TTF)$_2$IBr$_2$, τ = 10 ps [26]). In addition, for the generation of waves to be the most effective other conditions must be satisfied. This includes fulfillment of $k_s\delta_T << 1$ as long as the conditions for normal skin effect $l << \delta, \delta_T$ are satisfied. The Fermi velocity of β–(BEDT-TTF)$_2$IBr$_2$ is $v_F = 1.5 \cdot 10^5$ m/s [30] and the electron mean free-path is of order $l = v_F \tau$ = 1.5 μm. The skin depth of the β-(BEDT-TTF)$_2$IBr$_2$ crystals is about δ = 0.12 mm [30]. It is evident that the necessary conditions are fulfilled even at higher fields providing the ultrasound wave generation with double frequency to be studied experimentally in a wide range of magnetic fields. Experiments on thermoelectric generation of ultrasound waves in layered organic conductors

would be highly favorable since these compounds are synthesized with high purity that makes them very convenient for performing experiments.

4. CONCLUSIONS

The nonlinear generation of an ultrasound wave of double frequency ($\omega = 10^8$-10^9 Hz) in layered quasi-two dimensional organic conductors as a result of Joule heating as a heat source is considered. The amplitude of the generated wave due to thermoelectric stresses caused by the alternating part of the Joule heat is analyzed as a function of the magnetic field B, the angle between the normal to the layers and the magnetic field θ as well as of the characteristics of the conductor. Specifically, the parameters for the organic conductor β–(BEDT-TTF)$_2$IBr$_2$ are used to obtain the ultrasound wave amplitude $U_{2\omega}$ at temperature T = 30 K and the quasi-two dimensionality parameter $\eta = 10^{-3}$, i.e., for not strongly warped Fermi surface. It has been shown that the necessary conditions for observing the nonlinear generation of ultrasound wave with double frequency are always fulfilled even in relatively high but nonquantizing magnetic fields.

The oscillatory dependence of the ultrasound wave amplitude $U_{2\omega}$ on the angle θ is determined by the angular oscillations of the magnetoresistance $\rho_{zz}(\theta)$ which are associated with the charge carriers motion on the cylindrical Fermi surface in a tilted magnetic field. At angles where the amplitude $U_{2\omega}$ has maximum value, the average drift velocity $\bar{v}_z$ of charge carriers along the ultrasound wave vector coincides with the velocity s of the ultrasound wave and their interaction with the wave is most effective. Therefore narrow peaks appear in the angular dependence of the amplitude $U_{2\omega}$ that correspond to the most effective interaction of the charge carriers with the wave. From the period of the angular oscillations the diameter of the Fermi surface as well as the interlayer transfer integrals in the energy dispersion can be determined.

The magnetic field dependence of the amplitude $U_{2\omega}$ reveals existence of peaks present for small angles from the z-axis as well as for angles where the amplitude $U_{2\omega}$ has a dip in the angular dependence. The appearance of the peak in the field dependence could be associated with the resonant dependence of the ultrasound wave amplitude on magnetic field B at lower fields.

REFERENCES

[1] W. D. Wallace, Int. J. NDT **2**, 309 (1971)

[2] E. R. Dobbs, p. 127-150, in “Physical Acoustics. Principles and Methods”, Edited by W. P. Mason, Volume 10, Academic, New York (1973)

[3] H. M. Frost, pp. 179-275, in “Physical Acoustics”, Edited by W. P. Mason & R.N. Thurston, Volume 14, Academic Press, New York (1979)

[4] G. A. Budenkov and S. Yu. Gurevich, Defektroskopiya **5**, 5 (1981)

[5] A. N. Vasil'ev and Yu. P. Gaidukov, Usp. Fiz. Nauk **141**,431 (1983) [Sov. Phys. Usp. **26** (1 l), 952 (1983)]

[6] E. Kartheuser, R. L. Ram Mohan and S. Rodriguez, Adv. Phys. **35**,423 (1986)

[7] V. M. Kontorovich and A. M. Glushyuk, Zh. Eksp. Teor. Fiz. **41**, 1195 (1961) [Sov. Phys. JETP **14**(4), 852 (1962)]

[8] V**.** Ya. Kravchenko, Zh. Eksp. Teor. Fiz. **54**, 1494 (1968) [Sov. Phys. JETP **27**(5), 801 (1968)]
[9] V. L. Fal'ko, Zh. Eksp. Teor. Fiz. **85**, 300 (1983) [Sov. Phys. JETP **58**(1), 175 (1983)]
[10] A. N. Vasil'ev, Yu. P. Gaidukov, M. I. Kaganov *et al.,* Fiz. Nizk. Temp. **15**, 160 (1989) [Sov. J. Low Temp. Phys. **15**, 91 (1989)]
[11] G. Turner, R. L. Thomas and D. Hsu, Phys. Rev. B **3**, 3097 (1971)
[12] W. D. Wallace, M. R. Gaerttner and B. W. Maxfield, Phys. Rev. Lett. **27**, 995 (1971)
[13] D. E. Chimenti, C. A. Kukkonen and B. W. Maxfield, Phys. Rev. B **10**, 3228 (1974)
[14] D. E. Chimenti, Phys. Rev. B **13**, 4245 (1976)
[15] N. C. Banic and A. W. Overhauser, Phys. Rev. B **16**, 3379 (1977)
[16] E. A. Kaner, V. L. Fal'ko and L. P. Sal'nikova, Fiz. Nizk. Temp. **12**, 831 (1986) [Sov. J. Low Temp. Phys. **12**, 471 (1986)]
[17] E. Kartheuser and S. Rodriguez, Phys. Rev. B **33**, 772 (1986)
[18] M. A. Gulvanskii, Fiz. Tverd. Tela **29**, 1249 (1987) [Sov. Phys. Solid State **29**, 715 (1987)]
[19] Yu. I. Sazonov and Yu. M. Shkarlet, Defektoskopiya, No. 5, 1 (1969)
[20] I. Cap, Acta Phys. Slov. **32**, 77 (1982)
[21] A. P. Korolyuk and V. I. Khizhnyi, Pis'ma Zh. Eksp. Teor. Fiz. **48**, 348 (1988) [JETP Lett. **48**, 385 (1988)]
[22] A. N. Vasil'ev, M. A. Gulyanskii and M. I. Kaganov, Zh. Eksp. Teor. Fiz. **91**, 202 (1986) [Sov. Phys. JETP **64**(1), 117 (1986)]
[23] N. M. Makarov, F. P. Rodriguez and V. A. Yampol'skii, Zh. Eksp. Teor. Fiz. **95**, 205 (1988) [Sov. Phys. JETP **67**(9), 1943 (1988)]
[24] L. D. Favro, IEEE Ultrason. Symp. Proc. **1**, 399 (1986)
[25] A. A. Abrikosov, pp. 201-202, in “Fundamentals of the Theory of Metals”, Volume 2, North-Holland, Amsterdam (1988)
[26] M. V. Kartsovnik, Chem. Rev. **104**, 5737 (2004)
[27] D. Krstovska, O. Galbova and T. Sandev, EPL **81** 37006 (2008)
[28] K. Yamaji, J. Phys. Soc. Jpn. **58** 1520 (1989)
[29] R. Yagi, Y. Iye, T. Osada and S. Kagoshima, J. Phys. Soc. Jpn. **59** 3069 (1990)
[30] A. Chernenkaya, A. Dmitriev, M. Kirman, O. Koplak and R. Morgunov, Solid State Phenomena **190**, 615 (2012)

Институт за физика

Physica Macedonica **62**, (2016) p. 22-33

ON TWO EXTREMELY FAST METHODS FOR THE SOLUTION OF THE NON-LTE LINE FORMATION PROBLEM

O. Atanacković

Department of Astronomy, Faculty of Mathematics, University of Belgrade, Studentski trg 16, Belgrade, Serbia

Abstract. The solution of radiative transfer (RT) is a necessary step in the complex process of an astrophysical object modeling. In order to properly determine the physical and dynamical properties of an object from its spectrum, a reliable numerical method that can handle the multilevel non-LTE radiative transfer in spectral lines is needed. This problem is difficult to solve due to the non-local and strongly non-linear coupling between the atomic level populations (i.e. excitation state of the gas) and the radiation field intensities in the corresponding line transitions. For its solution an iterative method is required. For the solution of more complex, time-dependent or multi-dimensional RT problems, iterative method should be as fast as possible. Here we shall describe two methods, Iteration Factors Method (IFM) and Forth-and-Back Implicit Lambda Iteration (FBILI) that, owing to the use of the so called iteration factors in an explicit and implicit way respectively, converge extremely fast to the exact solution.

Key words: Radiative transfer, Numerical methods, Stellar atmospheres

1. INTRODUCTION

The spectra of astrophysical objects contain a wealth of information on their chemical composition and physical properties. The principal goal is to develop the methods to extract this information from their spectra. In practice, the so-called synthetic approach is applied: starting from the postulated model of an object and the theory of radiative transfer (RT) one computes the emergent spectrum and compares it to the observed one, produced by the real object and its own energy transport mechanisms. The model and the theory of radiation transport are to be modified until the agreement between the computed and the observed spectrum is reached. Therefore, the solution of radiative transfer in a given astrophysical object is an inevitable step in the object modeling.

The spectral lines are the best diagnostic tool for interpreting the physical properties of celestial bodies. Hence, the understanding of line formation, i.e. radiative transfer in spectral lines is of fundamental importance and deserves a special attention. We shall focus here on stellar spectra, since the stellar atmospheres are the most studied and the best understood astrophysical objects. However, the methods we consider here can be easily generalized to the study of RT in many other media.

At the beginning of the XX century and in the absence of advanced computational facilities, the simplifying physical models of line formation (e.g. pure absorption – LTE) had to be used. As the spectral lines are formed in the upper, low density regions of stellar atmospheres where radiative rates exceed the collisional ones and the scattering becomes important, in 1950's the picture of spectrum formation was greatly improved when the assumption of local thermodynamic equilibrium (LTE) was abandoned in favor of statistical equilibrium or the so-called non-LTE (NLTE). The intrinsic difficulty of the NLTE line transfer problem is in the non-local and generally non-linear coupling between the atomic level populations and the radiation field intensities in the corresponding line transitions. Scattering process makes the properties of very distant points in a medium non-locally coupled through the radiation field. The specific intensity of the radiation field at a given depth point depends, via the RT process, on the physical properties over a wide range of distant points. On the other hand, the physical state of the medium at each point depends, via radiative excitations and ionizations, on the radiation field itself. The dependence of the atomic level populations on the radiation field intensity is expressed by the statistical equilibrium (SE) or rate equations describing the balance between all the transitions (radiative + collisional) that populate and those that depopulate each given atomic level. From the mathematical point of view the coupling of the radiation field and the excitation state of the gas is described by the simultaneous solution of the corresponding equations of radiative transfer and statistical equilibrium.

If the line source function (the ratio of line emissivity to opacity) can be explicitly written in terms of the mean line radiation field intensity, as in the case of a two-level atom line transfer, the problem is linear and can be solved by using either direct or iterative methods. However, in the general case of a multi-level atom line transfer, the problem is highly non-linear and an iterative solution must be sought in order to solve the problem.

In what follows we shall first discuss the basic equations of the multilevel line formation problem (Sec.2), then the methods nowadays in use for its solution (Sec.3) and, finally, two such efficient, simple and fast convergent iterative methods that do not require any matrix formalism – Iteration Factors Method and Forth-and-Back Implicit Lambda Iteration (Sec.4 and 5) and, consequently, exhibit advantages in terms of stability, as well as considerable savings of both computational time and memory storage.

2. THE MULTI-LEVEL ATOM LINE FORMATION PROBLEM

For the sake of an easier presentation of the methods, here we shall consider the schematic case of a multi-level atom line formation in a plane-parallel, stationary medium of constant properties with complete redistribution and no background continuum. The three-level hydrogen atom is an ideal test case for checking the numerical accuracy and convergence properties of various algorithms developed to solve the RT problem, and its solution has been obtained by many authors (see e.g. [1]). Under the above assumptions, the RT equation for any line transition *ij* between two discrete energy levels *i* and *j* ($E_j > E_i$) takes the form

$$\mu \frac{d}{d\tau} I_{\nu\mu}(\tau) = \varphi_\nu [I_{\nu\mu}(\tau) - S(\tau)], \tag{1}$$

where $I_{\nu\mu}(\tau)$ is the specific intensity of the radiation field at the mean line optical depth τ, ν is the frequency and μ is the cosine of the angle between the direction of photon propagation and the outward normal. The absorption line profile φ_ν is assumed to be independent of both τ and μ. The line source function *S* contains the details of interactions between radiation and the atmospheric gas and depends on the populations of two bound atomic levels, *i* and *j*, the line transition is occurring between:

$$S = \frac{n_j A_{ji}}{n_i B_{ij} - n_j B_{ji}} = \frac{2h\nu^3}{c^2} \frac{1}{\frac{n_i}{n_j}\frac{g_j}{g_i} - 1}. \tag{2}$$

Here, B_{ij}, A_{ji} and B_{ji} are Einstein coefficients for absorption, spontaneous and stimulated emission, whereas g_i and g_j are statistical weights of the atomic levels. The level populations $\{n_i\}$ depend on the radiation field intensity through the statistical equilibrium (or rate) equations describing a balance between the processes that populate and depopulate a given atomic level. For each atomic level *j* of NL-level atom we have an equation of the form:

$$\begin{aligned} & n_j \{\Sigma(A_{ji} + B_{ji} J_\phi^{\ ij} + C_{ji}) + \Sigma(B_{jk} J_\phi^{\ jk} + C_{jk})\} \\ & = \Sigma n_i (B_{ij} J_\phi^{\ ij} + C_{ij}) + \Sigma n_k (A_{kj} + B_{kj} J_\phi^{\ jk} + C_{kj}) \end{aligned} \tag{3}$$

with $i < j$, $k > j$. Here, *C*'s are the inelastic collisional rates, while radiative rates contain the so-called scattering integrals

$$J_\phi^{\ ij}(\tau) = \int_{-\infty}^{\infty} \phi_\nu J_\nu(\tau) d\nu = \int_{-\infty}^{\infty} \phi_\nu d\nu \frac{1}{2} \int_{-1}^{1} I_{\nu\mu}(\tau) d\mu \tag{4}$$

that account for the angle and frequency coupling of the specific intensities at the given depth point. For the NL-level atomic model, NL-1 linearly independent SE equations are closed by the particle conservation equation:

$$\sum_i n_i = n_{tot} \tag{5}$$

where n_{tot} is the total number density of atoms.

3. NUMERICAL METHODS FOR THE SOLUTION OF MULTI-LEVEL PROBLEM

The above non-linear problem requires a simultaneous solution of the RT and SE equations, which can be achieved only through iterations. Various methods differ in the way linearity is achieved at each iterative step. The first robust method that could handle mutual non-

linear coupling of all relevant variables in a fully self-consistent manner was the complete linearization (CL) method by Auer and Mihalas [2]. The coupled equations are linearized in all variables and solved simultaneously for the variables' corrections. The convergence rate of the CL method is very high. However, as a very large number of frequency, angle and depth points is usually needed for a good description of the physical system, huge memory storage and a lot of computing time are required. Moreover, the optimization of this *global* method is rather difficult.

Much simpler and cheaper methods were needed to solve more realistic and complex problems. These are the methods that use a *sequential* iterative procedure within the so-called *structural* approach (Simonneau and Crivellari [3]). They take advantage of the fact that a problem can be divided into separate tasks according to the physics of the problem and the mathematical properties of the relevant equations. The current solution of each individual task is obtained by assuming that the output of the others is known. Thus each task can be optimized independently. More specifically, in the multilevel line formation problem, each step of the iterative procedure is usually split in two parts so that within each of them, one of the two systems of equations, RT and SE, is solved by taking the solution, or part of the solution, of the other one as known. The coupling is performed at the end of the iterative procedure, with the convergence rate that depends on the amount of information transferred between the two parts.

The simplest and the well-known sequential iterative procedure is Λ iteration that solves the problem equations in turn. However, in scattering-dominated media of large optical thickness (typical non-LTE conditions), the convergence of Λ iteration is extremely slow. It follows the process of a particular scattering event and at each iteration step it corrects the solutions only within a unit optical path. It transfers from one part of the iterative step to the other more information than necessary.

There are two broad classes of methods attempting to facilitate the solution of NLTE line transfer problem and improving upon the difficulties encountered by the above mentioned methods. One is based on the so-called ETLA (Equivalent-Two-Level-Atom) approach, described in [4], in which only one transition in the atomic model at a time is combined with the transfer problem, whereas the coupling of all levels is achieved by iteration over all transitions. However, it may happen that iterative procedure converges upon inconsistent solutions as the multilevel transition interlocking is treated iteratively. The other approach employs an approximate treatment of RT coupled with the full set of SE equations. The exact Λ operator is replaced by an approximate one, whereas a small error introduced by this approximation is accounted for iteratively. The approximation is based either on the physics of the transport of photons through the medium (escape probability, core saturation etc.) or on some computational considerations. Such approach is known as ALI (Approximated/Accelerated Lambda Iteration). Rybicki [5] and Cannon [6] pioneered the first ideas of ALI methods. Rybicki eliminated the cause of the slow convergence of simple Λ iteration, i.e. poor conditioning of the equations arising from a large number of scatterings, by the elimination of scatterings in the line core (core saturation assumption) which do not contribute much to RT. The solution of the *preconditioned* equations that contain only wing components by direct Λ iteration converged more rapidly. Cannon was the

first to use the idea of 'operator splitting' from the numerical analysis in radiative transfer computations. He replaced the full (exact) Λ operator by the so called approximate Lambda operator - ALO and computed a small error term made by this approximation using a perturbation technique. His ALO was Λ operator evaluated with fewer angular-frequency quadrature points.

ALO has to be simpler to invert than the Λ operator, and also as close physical approximation of the exact Λ operator as possible to ensure stable and rapid convergence to the exact solution. Olson et al. [7] were the first to point out that the diagonal (local) part of the exact Λ matrix represents nearly optimum approximate operator. The most commonly used ALI method is the Jacobi iteration scheme that employs the diagonal ALO and computes the error introduced by this approximation iteratively. Using a 'short characteristic' solution of the first-order differential RT equation and parabolic approximation for the source function Olson and Kunasz [8] derived a fast method to compute the exact diagonal of the Λ matrix. The approach that introduces ALO directly into SE equations to make them linear from the outset (preconditioning) is proposed by Rybicki and Hummer [9]. This is the well-known MALI (Multilevel Accelerated Lambda Iteration) method, which was successfully applied to the solution of various RT problems. The convergence rate of the Jacobi method is usually increased by the Ng acceleration technique [10]. The diagonal ALO is also used as the local-operator option of the well-known multilevel transfer code MULTI [11].

Another numerical method for NLTE RT applications that is twice as fast as the Jacobi method is the Gauss-Seidel (GS) method by Trujillo Bueno and Fabiani Bendicho [12]. Its implementation into multilevel RT is made explicit by Paletou and Leger [13]. Successive Overrelaxation (SOR) is applied to speed up its convergence. The use of additional mathematical techniques is not straightforward. It usually needs some preliminary analyses in order to prevent the divergence of the whole procedure. Therefore, despite important progress made thanks to ALI methods, the search for more efficient algorithms is still an open field of research.

Another approach that uses the so-called iteration factors, either in explicit or implicit way, is implemented in two extremely fast methods: the Iteration Factors Method (IFM) and the Forth-and-Back Implicit Lambda Iteration (FBILI), respectively. These are the methods developed for the NLTE line transfer problem by Atanackovic-Vukmanovic [14], Atanackovic-Vukmanovic and Simonneau [15], Atanackovic-Vukmanovic, Crivellari and Simonneau [16] and Kuzmanovska-Barandovska and Atanackovic [17]. They will be discussed here in more details.

4. ITERATION FACTORS METHOD

As we have already emphasized, a global astrophysical problem can be divided into several specific physical key-problems represented by individual blocks of a general block-diagram. The optimum structure of the block-diagram is determined by the physics itself. A current solution of each block is obtained assuming that the output from all the others is known. The solution of the global problem is thus achieved through a sequential iterative procedure. The most straightforward Λ iteration scheme is very slow. However, its slight modification can lead to an *extremely high* convergence rate. One such revision is in the use of the so-called iteration

factors (IFs) as the input/output of the blocks that constitute the block diagram. At each iteration step the IFs are computed from the current solution and then used to update it. In order to provide fast convergence they have to be good quasi-invariants (to change little from one iteration to another). Because being defined as the ratios of the homologous physical quantities, they become exact already in the first few iterations leading quickly to the exact solution of the whole procedure.

In RT literature, the idea of iteration factors appeared for the first time in the paper by Feautrier [18] who suggested that the use of the ratio of two moments of the radiation field intensity could speed up the stellar atmosphere model computations. The first realization of the idea was the variable (depth-dependent) Eddington factor (VEF) technique [19] developed for the solution of the monochromatic transfer problem in plane-parallel geometry (Fig.1). Auer and Mihalas iterated on the ratio of the third to the first angular moments of the radiation field $F=K/J$, i.e. on the so-called Eddington factor.

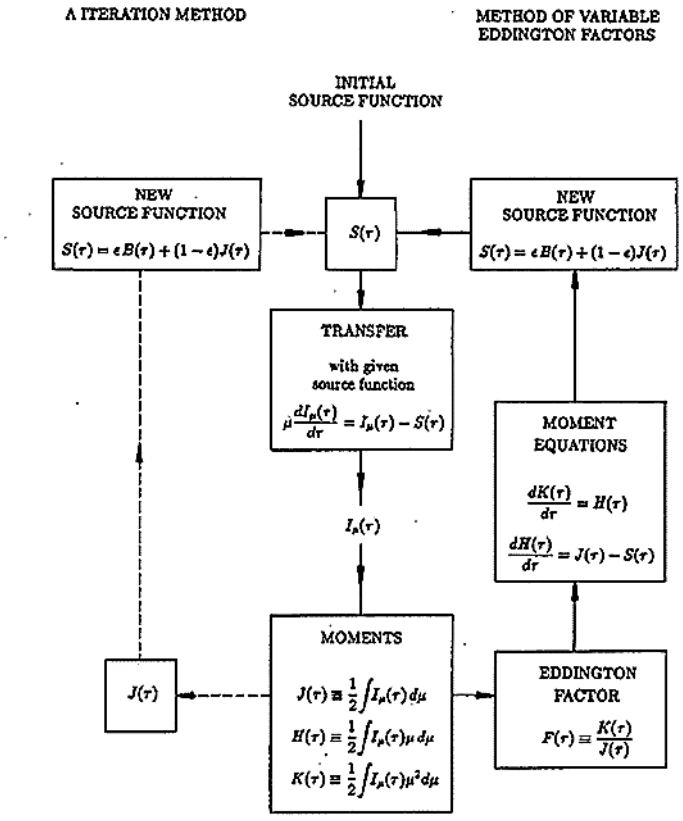

Figure 1. Flow-chart of the method of VEFs for the monochromatic transfer problem.

They pointed out that it is much better to iterate on the ratio of two quantities than on the quantities themselves, as their ratio changes much less from one iteration to another. An extremely fast convergence is achieved at the cost of a small additional effort, with respect to the Λ iteration, of iterative computation of Eddington factor and the solution of one second-order differential equation (i.e. two first-order differential equations closed by the iteration factor, see Fig.1). Two to three iterations were enough to reach the exact solution.

The VEFs have been applied within the linearization method for both, the stellar atmosphere modeling [2] and the line formation [20], problems to reduce the angular dimensions of the system under study. They enabled a complex explicit frequency-angle coupling to be simplified, so that only the frequency coupling is treated explicitly, whereas the angle coupling is treated iteratively. However, a very large number of frequency points still made the computations with the CL/VEF demanding.

The idea of VEFs is generalized in the Iteration Factors Method (IFM), developed to solve the two-level-atom line transfer problem by Atanackovic-Vukmanovic [14] and Atanackovic-Vukmanovic and Simonneau [15]. For the first time they used both angle and frequency averaged iteration factors, defined for a line as a whole. At each iteration, depth-dependent factors defined as the ratios of the relevant (angle and frequency) intensity moments are computed from the current values of the radiation field and then used to close the system of the RT equation moments. The iteration factors method does not need any matrix operation, thus requiring small memory storage and computational time.

The IFM is extended to the solution of the multilevel line transfer problem by Kuzmanovska-Barandovska and Atanackovic [17]. Iterative procedure that overcomes the above mentioned drawback of the CL/VEF method is proposed, retaining its favorable convergence properties while becoming computationally cheap owing to the use of iteration factors defined for each line as a whole. The algorithm is displayed in Fig.2.

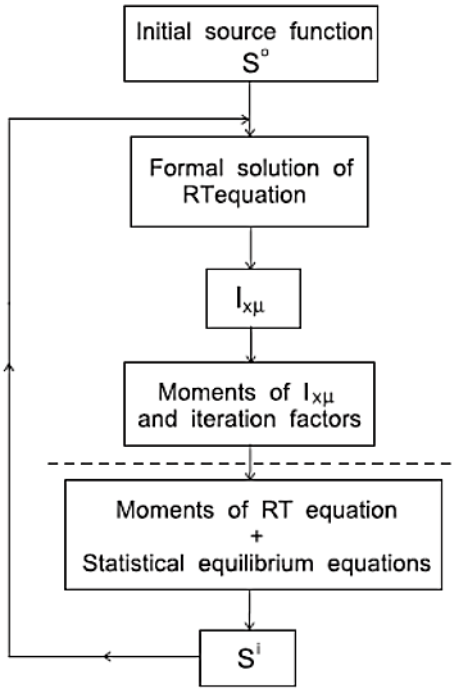

Figure 1. Flow-chart of the IFM for the line transfer problem. The algorithm is divided by dashed line in two parts that can be optimized independently.

In the first part of each iteration, starting from a given source function (S^0) or the one known from the previous iteration step (S^i) we formally solve the RT equation (1) for each line

transition. The obtained intensities are used for the computation of the relevant angle and frequency integrated moments and the iteration factors as their ratios. The IFs are then used as the known coefficients to close the system of the RT equation moments (for all line transitions) non-linearly coupled with the statistical equilibrium (SE) equations (for all level populations) and to update the solution in the second part of each iteration. Two approaches were used to solve these two systems of equations simultaneously. The first one is based on the *linearization* of the equations by neglecting the second- and higher-order terms. A substitution of the linearized SE equations into the linearized RT equation moments yields the system of equations that involve only the corrections of the frequency integrated mean intensity of the radiation field explicitly. In the second approach, the linear form of the SE equations is obtained by assuming that the level populations in their line-opacity-like terms are known from the previous iteration. Thus one derives linear relations between each line source function and the full set of the radiation field mean intensities and solves them together with the RT equation moments for all line transitions linearly coupled in this way. The second approach can be labeled "*preconditioning*". In both approaches an extremely fast convergence is provided and the cost per iteration drastically reduced by the use of quasi-invariant iteration factors in the linearly coupled RT equation moments and SE equations.

The proposed method is tested on a standard benchmark model for the multilevel atom problems: three-level hydrogen atoms in a plane-parallel, semi-infinite isothermal atmosphere with no background opacity. We compared the convergence rate of the IFM with that of the MALI method, using the results given in [9]. The convergence rate of the IFM is higher than that of MALI by a factor of more than 5 with respect to the solution with diagonal operator without acceleration (D/N), and by a factor of about 2 for the tridiagonal ALO without acceleration (T/N). Only the use of tridiagonal ALO with Ng acceleration (T/A) provided more rapid convergence than the IFM (that uses no additional acceleration). In Table 1. the convergence properties of the IFM are compared with those of the methods currently in use (MALI, Gauss-Seidel and SOR), the results of which for the same test problem are given by Paletou and Leger [13]. One can see that the total computational work (CW) of the IFM is 5-6 times lesser than that of MALI. IFM is about 4 times faster than GS and 1.5 times faster than GS accelerated by SOR.

Table 1: Comparison of the convergence properties of the IFM with other methods (MALI, GS and SOR [13]). Iter – number of iterations needed to satisfy a given R_c (maximum relative change of the source function between two successive iterations), CPU/Iter – computational time per iteration and CW – total computational work.

R_c	**MALI**			**GS**			**SOR**			**IFM**		
	Iter	**CPU/Iter**	**CW**	**Iter**	**CPU/Iter**	**CW**	**Iter**	**CPU/Iter**	**CW**	**Iter**	**CPU/Iter**	**CW**
10^{-2}	100	0.163	16.3	55	0.21	11.6	25	0.21	5.25	12	0.238	2.86
10^{-3}	170	0.163	27.7	85	0.21	17.9	35	0.21	7.35	19	0.238	4.52
10^{-4}	230	0.163	37.5	120	0.21	25.2		0.21	8.40	26	0.238	6.19

Very high convergence rate is not affected by the refinement of the grid resolution, i.e. the number of iterations is practically insensitive to the spatial grid, so that the total computational

work scales linearly with the number of depth grid points (see Table 2). As an additional check the IFM was applied to the solution of a 5-level CaII ion model, the test problem proposed by Avrett [21], and similar, very encouraging results are obtained [22].

5. FORTH-AND-BACK IMPLICIT LAMBDA ITERATION

Another simple and efficient method developed to accelerate the convergence of the classical Λ-iteration while retaining its straightforwardness is Forth-and-Back Implicit Lambda Iteration – FBILI [14, 16]. It makes use of the fact that even if the radiation field is not known, its physical behavior can be easily represented. An implicit representation of the source function is used in the computation of both the in-going ($I_{\nu\mu}^{\ -}$) and the out-going ($I_{\nu\mu}^{\ +}$) intensities of the radiation field that are considered separately within a forth-and-back approach. Namely, using the integral form of the RT equation

$$I_{\nu\mu}^{\ -}(\tau_l) = I_{\nu\mu}^{\ -}(\tau_{l-1})e^{-\Delta\tau\varphi_\nu/\mu} + \int_{\tau_{l-1}}^{\tau_l} S(t)e^{-(\tau_l - t)\varphi_\nu/\mu}\frac{\varphi_\nu}{\mu}dt$$

$$I_{\nu\mu}^{\ +}(\tau_l) = I_{\nu\mu}^{\ +}(\tau_{l+1})e^{-\Delta\tau\varphi_\nu/\mu} + \int_{\tau_l}^{\tau_{l+1}} S(t)e^{-(t-\tau_l)\varphi_\nu/\mu}\frac{\varphi_\nu}{\mu}dt \qquad (6)$$

and assuming polynomial (e.g. piecewise parabolic) behavior for the source function in each depth subinterval $\Delta\tau$, for every optical depth point τ_l one can write implicit linear relations representing the specific intensities in terms of the yet-unknown values of the source function and its derivatives:

$$I_{\nu\mu}^{\ \pm}(\tau_l) = a_{\nu\mu}^{\ \pm} + b_{\nu\mu}^{\ \pm}S(\tau_l) + c_{\nu\mu}^{\ \pm}S'(\tau_l) \qquad (7)$$

According to the idea of iteration factors, the iterative computations of the coefficients of these implicit relations (implicit, as the source function is *a priori* unknown), rather than of the unknown functions themselves, greatly accelerate the convergence of the iterative scheme. The coefficients are computed layer by layer during the forward ('in-going') elimination process and stored for further use in the back substitution process when the explicit values of unknown functions are computed.

In more detail, proceeding from the upper boundary condition and using an initial estimate of the source function (or that known from the previous iteration step) one can compute and store, at all optical depths, the coefficients of the linear relation for the in-going specific intensities:

$$I_{\nu\mu}^{\ -}(\tau_l) = \left(\frac{a_{\nu\mu}^{\ -}}{S^0(\tau_l)} + b_{\nu\mu}^{\ -}\right)S(\tau_l) + c_{\nu\mu}^{\ -}S'(\tau_l), \qquad (8)$$

where $a_{\nu\mu}^{-}$ is to be computed with old (from the previous iteration) source function. Finally, the coefficients of the linear relation for the unknown in-going mean radiation field

$$J_{\varphi}^{-}(\tau_l) = b_l^{-} S(\tau_l) + c_l^{-} S'(\tau_l), \tag{9}$$

are stored.

The aim is to obtain the coefficients of the linear relation between the 'full' mean intensity and the source function ($J_{\varphi} = a + bS$) which, when substituted into the statistical equilibrium equations, lead to the new source function. In order to obtain the 'full' coefficients a and b, the coefficients of the corresponding implicit relation for the out-going mean intensities are needed. Proceeding from the lower boundary condition we determine them simultaneously with the updated source function when sweeping layer by layer back to the surface. The process is iterated to convergence. A negligible additional computational effort made within FBILI method with respect to the classical Λ iteration results in an extremely fast convergence to the exact solution. This is due to the fact that the only information transferred from the previous iteration step to the next one is in the ratio between the non-local part of the inward mean intensities and the current (old) source function ($a_{\nu\mu}^{-} / S^{0}$), which represents an iteration factor.

The efficiency and the accuracy of the FBILI method have been verified on several RT problems. The two-level-atom line transfer problem with complete redistribution (CRD) and its generalization to the case of partial frequency redistribution (PRD), as well as the multi-level-atom line formation problem with CRD, are considered by Atanacković-Vukmanović, Crivellari and Simonneau [16]. The exact solutions are obtained in a very small number of iterations even under extreme non-LTE conditions. The method is generalized to the monochromatic scattering and two-level atom line formation in static spherical media [23, 24], to the two-level line formation in media with low velocity fields [25] and to the two-level line formation in 2D Cartesian coordinates [26]. The multi-level atom line transfer in 1D is made more explicit in [27]. In Table 2, the comparison of the convergence properties of IFM and FBILI methods is shown. The CPU time per FBILI iteration is only 10% longer than CPU per Λ iteration. In terms of the total computational work, FBILI is faster than IFM by a factor of 2. Both methods have higher convergence rate than those currently in use (see Tables 1 and 2). Another important advantage of the two methods with respect to the ALI ones is that their total CW scales linearly with the number of grid points.

Table 2: Convergence properties of the IFM and FBILI methods: the number of iterations (Iter) required to satisfy the criterion $R_c = 10^{-4}$, the computation time per iteration (CPU/Iter) in seconds and total computational work (CW) for the three-level H atom benchmark problem as a function of the number of depth points per decade N_{τ}.

N_{τ}	**Λ iteration**	**IFM**			**FBILI**		
	CPU/Iter	**Iter**	**CPU/Iter**	**CW**	**Iter**	**CPU/Iter**	**CW**
3	0.0135	23	0.0183	0.422	11	0.0156	0.172
6	0.0264	23	0.0353	0.813	15	0.0292	0.438
9	0.0395	28	0.0525	1.469		0.0436	0.828

6. CONCLUSIONS

In order to speed up the convergence, the iterative methods nowadays in use to solve various RT problems usually employ some additional mathematical acceleration techniques, the implementation of which is not straightforward and may lead to divergence of the iterative procedure. We have shown that the use of iteration factors (either explicitly – Iteration Factors Method, or implicitly – Forth-and-Back Implicit Lambda Iteration) enables an extremely fast convergence to the exact solution of NLTE radiative transfer problems with no need for an extra acceleration.

In particular, the advantages of the IFM with respect to the CL and ALI methods are as follows: (1) the iteration factors defined for line as a whole reduce drastically the need for large memory and computing time and (2) there is no increase in the number of iterations with the grid resolution refinement. The FBILI method is even more simple, stable and extremely fast. The facts that it is a two-point algorithm and that the memory storage grows linearly with the dimensions of the problem makes FBILI very suitable for 3D RT.

Both methods are rapidly converging, exact and stable, being thus very promising in the applications to more complex problems, in which RT is coupled with other physical phenomena.

ACKNOWLEDGEMENTS

This work has been realized within the project No. 176004 (”Stellar Physics”) supported by the Ministry of Education, Science and Technological Development of the Republic of Serbia.

REFERENCES

[1] E.H. Avrett and R. Loeser, in Numerical Radiative Transfer, ed. W. Kalkofen (Cambridge Univ. Press), p. 135 (1987)

[2] L.H. Auer and D. Mihalas, Astrophys. J. **158**, 641-655 (1969)

[3] E. Simonneau and L. Crivellari, Structural algorithms to solve radiative transfer problems, Research Project, Instituto de Astrofisica de Canarias (1994)

[4] D. Mihalas, Stellar Atmospheres, 2nd edition, Freeman, San Francisco (1978)

[5] G. Rybicki, in: R.G. Athay, L.L.House, G.Jr Newkirk, editors. Line formation in the presence of magnetic fields. High Altitude Observatory, Boulder; p.145 (1972)

[6] C.J. Cannon, Journal of Quant. Spectrosc. Radiat. Transfer **13**, 627-633 (1973)

[7] G.L. Olson, L.H. Auer, J.R. Buchler, Journal of Quant. Spectrosc. Radiat. Transfer **35**, 431-442 (1986)

[8] G.L. Olson and P.B. Kunasz, Journal of Quant. Spectrosc. Radiat. Transfer **38**, 325-336 (1987)

[9] G. Rybicki and D. Hummer, Astron. Astrophys. **245**, 171-181 (1991)

[10] K.C. Ng, J. Chem. Phys., **61**, 2680-2689 (1974)

[11] M. Carlsson, A Computer Program for Solving Multi-Level Non-LTE Radiative Transfer Problems in Moving or Static Atmospheres, Uppsala Astron. Obs. Rep. 33, (1986, 1991)

[12] J. Trujillo Bueno, P. Fabiani Bendicho, Astrophys. J. **455**, 646-657 (1995)

[13] F. Paletou, L. Leger, Journal of Quant. Spectrosc. Radiat. Transfer **103**, 57-66 (2007)

[14] O. Atanacković-Vukmanović, PhD thesis, Department of Astronomy, Faculty of Mathematics, University of Belgrade (1991)

[15] O. Atanacković-Vukmanović, E. Simonneau, Journal of Quant. Spectrosc. Radiat. Transfer **51**, 525, (1994)
[16] O. Atanacković-Vukmanović, L. Crivellari and E. Simonneau, Astrophys. J. **487**, 735-746 (1997)
[17] O. Kuzmanovska-Barandovska and O. Atanacković, Journal of Quant. Spectrosc. Radiat. Transfer **111**, 708-722 (2010)
[18] P.Feautrier, C.R.Acad.Sci., Paris, **258**, p. 3189 (1964)
[19] L.H. Auer, D. Mihalas, MNRAS **149**, 65 (1970)
[20] L. Auer, Astrophys. J. **180**, 469-472 (1973)
[21] E.H. Avrett, Resonance Lines in Astrophysics, National Center for Atmospheric Research, Boulder, 27 (1968)
[22] O. Kuzmanovska-Barandovska and O. Atanacković, Publ. Astron. Obs. Belgrade **90**, 155-158 (2010)
[23] O. Atanacković-Vukmanović, Serb. Astron. J. **167**, 27-34 (2003)
[24] O. Atanacković-Vukmanović, ASP Conference Series **370**, 97-102 (2007)
[25] I. Pirković and O. Atanacković, Serb. Astron. J. **189**, 53-67 (2014)
[26] I. Milić and O. Atanacković, Advances in Space Research **54**, 1297-1307 (2014)
[27] O. Kuzmanovska, O.Atanacković and M. Faurobert, in preparation (2016)

Институт за физика

Physica Macedonica **62**, (2016) p. 34-40

METHOD OF ABSOLUTE GRAVITY MEASUREMENT AND ITS INFLUENCE IN MASS DETERMINATION

Luljeta Disha[1], Defrim Bulku[1] and Antoneta Deda[2]

[1]*General Directorate of Metrology, Autostrada Tr-Dr, km 8, Kashar,1000 Tirana, Albania*

[2] *Faculty of Natural Science, Bulevardi Zogu I, 1000 Tirana, Albania*

Abstract. The determination of acceleration due to gravity has application in many measurements. Its value is of interest in a broad area of physical sciences, Metrology, Geophysics and Geodesy. In Metrology, knowledge of the gravity field is very important in mass determination, and also it is used as a transfer standard in the determination of metrological standards involving force and pressure measurements. The need for modern absolute gravity measurements within 10^{-9} relative uncertainty is one of the priority tasks in metrology. This paper describes the determination of acceleration due to gravity using IMGC-02 absolute gravimeter and its influence on a weighing result. The instrument adopts the symmetric-free fall method where both the rise and falling trajectory is used to fit the motion model. The trajectory of the flying object is recorded interferometrically by measuring the distance over which it moves with the wavelength of a He-Ne laser. The results of absolute gravity measurements are carried out in the gravity laboratory of National Institute of Metrological Research, (INRIM) Turin, Italy in collaboration with the gravimetry field staff. In the paper are also presented some applications in determination of acceleration due to gravity in mass field.

PACS: pacs 04.80.Nn, pacs 06.20 F, pacs 06.20.fb, pacs 06.30.Dr

1. INTRODUCTION

Since the absolute gravity varies with both position and time, metrological use of gravity as a constant, requires that it is measured wherever it is needed and if the accuracy requirements are higher than 10^{-8}, it will be necessary to measure it also at the time it is needed. The accuracy requirements differ considerably and are strongly related to the purpose of the research. Metrology, related to standards of force and pressure, needs to know "*g*" with accuracy of the order of 10^{-6}-10^{-7}. For Mass Metrology, order of magnitude for "*g*" is required to be between 10^{-8}-10^{-9}. Hence the need of high-precision measurement of "*g*", which can be achieved only by means of the modern absolute gravimeters, is very essential. The local "*g*" value is extracted from the trajectory of a free falling test body by fitting a suitable motion model to the time-space coordinates. In order to establish the accuracy in "g" measurements, it is needed for the traceability to the primary standards of the length and time units. Such accuracy is reached by using optical interferometric methods to track the test mass flight. In the IMGC-02 instrument developed in INRIM an atomic clock (Rubidium) and primary He-Ne stabilized laser guarantee the traceability in time and length [1]. This apparatus has been part of some International

Comparisons of Absolute Gravimeters and has achieved very good results showing the good reproducibility of the apparatus. The influence of absolute gravity in the indication of a weighing instrument of class II is reported for two different places in Albania.

2. METHOD AND EQUIPMENT

In nowadays the best accuracy achievable in measuring the absolute gravity, concerns instruments which adopt the so called ballistic method which is recognized by the International Committee of Weights and Measurements (CIPM), as primary method. It is some microgal (1 μGal = 1×10^{-8} m·s^{-2}). The IMGC-02 instrument adopts the symmetric-free fall method where a corner-cube prism is thrown up vertically in a vacuum chamber about 20 cm [1]. Interference fringes emerging from the interferometer are detected by a photo-multiplier. The raw datum consists in an array, where each element represents the time correspondent to the passage of the test-body through equally spaced stations. A useful motion model is fitted to the time-position coordinates in a total least-squares algorithm. One of the estimated parameters of the model is the acceleration due to gravity experienced by the test-body during the flight. A photo of the measuring system of IMGC-02 absolute gravimeter and the test mass is reported in figure 1.

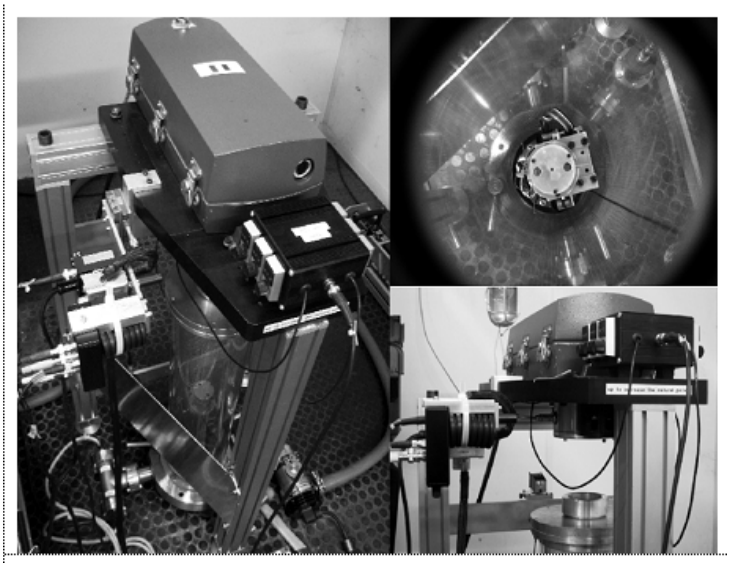

Figure 1. Measuring system of IMGC-02 absolute gravimeter

The complete automation of the instrument allows a measurement rate of about 120 launches every hour. The measurement uncertainty is a combination of effects due to influence factors characteristic of the instrument, together with the effects characteristic of the observation site. We can mention here the laser beam verticality and divergence, fringe timing, tide, polar motion, Coriolis force, self-attraction etc. It is evaluated as the combined standard uncertainty times the coverage factor at the 95% confidence level. The experimental results of "*g*" value performed with IMGC-02 absolute gravimeter in the gravity laboratory in INRIM from 17.02.2014 - 20.02.2014 are reported in figure 2.

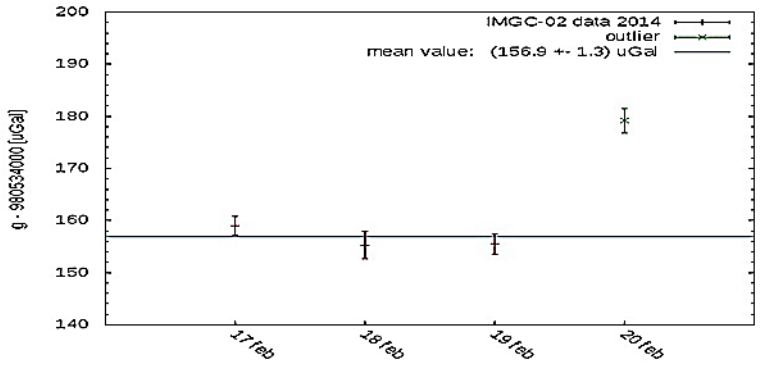

Figure 2. Measurement carried out in INRIM laboratory for four days.

3. APPLICATIONS ON DETERMINATION OF ACCELERATION DUE TO GRAVITY

3.1 Mass determination of the standards weights

For many years National Metrology Institutes (NMIs) as well as the BIPM have made considerable efforts to advance and improve the SI units. Progress is being made towards a redefinition of Kilogram realizing experiments based on a constant of nature. Among them is an electro-mechanical experiment realized via the Watt Balance which tries to link the Kilogram to the Planck constant (h). In this experiment the *"g"* measurement has fundamental importance and the required uncertainty is below 5×10^{-9}.

Since the unit of mass is only available at the BIPM, it must be disseminated to the rest of the world through a series of comparison calibrations involving national prototypes. The unit of mass is then disseminated in each country from Pt-Ir kilograms to a mass scale covering multiples and submultiples of the kilogram.

In this way, at the highest level of mass measurement, the comparison between a Pt-Ir mass standard and stainless steel kilograms, determination of acceleration due to gravity is essential. Due to the vertical gradient of the gravitational acceleration, different levels of the centre of gravity of reference standard and test object exert an influence in very precise mass determination (also in hydrostatic weighing)

$$y = \Delta m + \rho_a \left(V_{Tt} - V_{St} \right) + C_{ml} , \tag{1}$$

where:

y - is the mass differences obtained by weighing

Δm - is the difference of balance readings calculated from weighing cycles (ABBA)

ρ_a - air density at the time of the weighing

V_{Tt}, V_{St} - volumes of the weights involved (test and standard respectively) in a measurement at temperature "t",

C_{ml} - is the correction due to different centre-of-mass levels calculated as [2, 3]:

$$C_{ml} = m\,\gamma\,\frac{\delta h}{g}, \tag{2}$$

where:

m - nominal value of the weight

γ - gravitational gradient

g - acceleration due to gravity

δh - represents the distance between the centres of mass of the two artefacts being compared

Mass laboratory of General Directorate of Metrology in Albania (DPM) periodically ensures the traceability of mass unit in INRIM and Physikalisch-Technische-Bundesanstalt (PTB) Germany. These two NMIs provide their traceability of mass unit at the BIPM.

3.2 Calibration of Non Automatic Weighing Instrument (NAWI)

Inaccurate measurements in scales or in the weighing operation during trading causes unfair trade transactions. Acceleration due to gravity is very essential in the process of calibration of the weighing instruments. The indication of an instrument is proportional to the force exerted by an object of mass *m* on the load receptor [4].

$$I = m\,g\left(1-\frac{\rho_a}{\rho}\right)k_s, \tag{3}$$

where:

g - local acceleration gravity

ρ_a - density of the surrounding air

ρ - object density

k_s - adjustment factor

Normally the calibration of a weighing instrument must be performed in the location where the instrument is being used. The electronic reading balance takes measurement of mass making use of absolute gravity "g". Difference in geographic region and altitude, influence in the gravity acceleration. Therefore for obtaining accurate measurements, it is mandatory to adjust the scale to the local environment. Standard weights used for the adjustment of weighing instruments must have been calibrated to the conventional value of mass m_c and traceable to the International System of Units (SI).

In order to see the differences in mass readings there are performed measurements using a weighing instrument of class II, in two different places in Albania. In table 1and 2 are reported the indication values of the weighing instrument before and after the adjustment process respectively in Tirana and Vlore. The weighing instrument belongs to a customer of Mass

Laboratory in Albania which has requested a calibration for this instrument after it has changed the place of use from Tirana to Vlore.

Table 1: Values of weighing instrument indication and error before and after adjustment in Tirana

Nominal Value (g)	Indication before adjustment (g)	Error of indication (g)	Indication after adjustment (g)	Error of indication (g)
1	0.97	-0.03	0.99	-0.01
1000	999.90	-0.10	1000.00	0.00
2000	1999.79	-0.21	1999.98	-0.02
3000	2999.69	-0.31	2999.97	-0.03
4000	3999.53	-0.47	3999.92	-0.08

It can be seen that for the maximum load before adjustment process the indication error is in the range 4.7 $x10^{-1}$ g and after the adjustment process the error of indication for the weighing instrument is in range 8.0 $x10^{-2}$ g. Thus for the same nominal mass, indication of the balance has a considerable difference. Figure 3 shows the errors of balance indication before and after adjustment and the linear approximation equation of these errors.

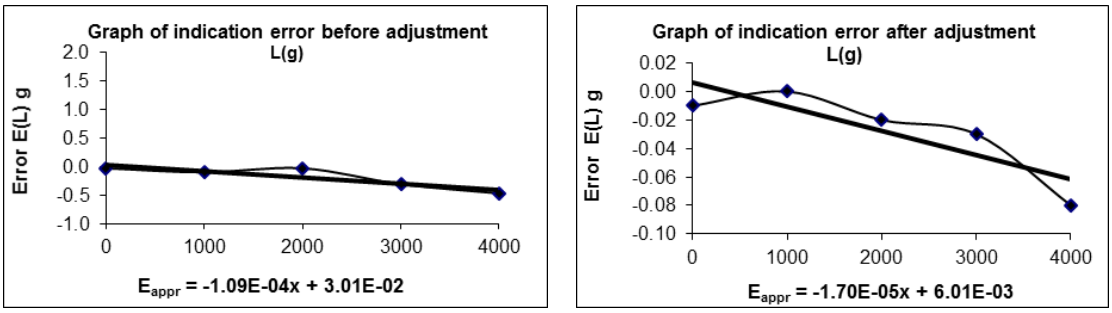

Figure 3. graphs of the errors of balance indication before and after adjustment and the linear approximation equation of these errors.

When this instrument is displaced to Vlore, the values of weighing instrument indication and the errors of indications are as reported in table 2. The graph is reported in figure 4.

Table 2: Values of weighing instrument indication and error before and after adjustment in Vlore

Nominal Value (g)	Indication before adjustment (g)	Error of indication (g)	Indication after adjustment (g)	Error of indication (g)
1	0.98	-0.02	1.00	0.00
1000	999.85	-0.15	999.98	-0.02
2000	1999.70	-0.30	1999.98	-0.02
3000	2999.58	-0.42	2999.98	-0.02
4000	3999.41	-0.59	3999.96	-0.04

In the same way it can be seen that for the maximum load before adjustment process the indication error is in the range 5.9 $x10^{-1}$ g and after the adjustment process the error of indication for the weighing instrument is in range 4 $x10^{-2}$ g. The same as in Tirana, the indication of the

balance has a considerable difference. This phenomenon is due to the difference in gravitational acceleration resulting from the difference in geographic region and height above sea level.

In other words, a sensitivity error occurs, the balance measurement values become smaller as it is moved from Tirana to Vlore.

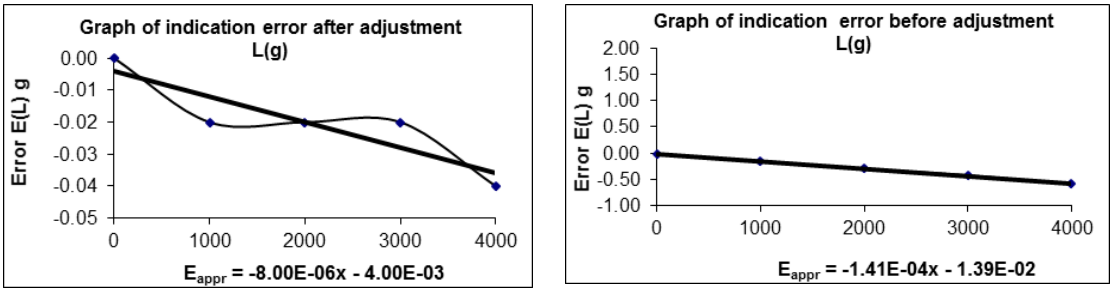

Figure 4. Graphs of the errors of the weighing instrument indication, before and after adjustment in Vlore.

In both cases the uncertainty of measurement is approximately the same. It is in the range 10^{-1} g. It means that variation of "*g*" value in terms of errors of indication is very important, while in terms of uncertainty of measurement it has not a significant contribution.

In order to optimize the conventional mass of the instrument indication normally it is better to perform the adjustment process before the calibration of the weighing instrument. A weighing instrument should not be displaced to another location after the calibration, as the performance of the instrument alter and may invalidate the calibration because of the difference in local gravity acceleration.

3.3 Verification of Non Automatic Weighing Instrument (NAWI)

Weighing instruments of medium or higher accuracy which normally use strain-gauge load cells are used a lot in industry and trade for commercial transactions. Thus from the legal point of view the adjustment by an external weight at the place of use is normally not allowed for the user, but only for an authorized person. European regulations foresee verification in two stages: the first one comprising all examinations that are gravity-independent, which can be carried out at the manufacturers' works, and a second one, comprising essentially the final adjustment by an authorized person at the place of use. For the verification process of NAWI the maximum permissible variation Δg/g is calculated using the criterion [5]:

$$\frac{\Delta g}{g} \leq \frac{mpe}{3ne} \tag{4}$$

where:

Δg/g - is the allowed relative variation of gravity acceleration
mpe - is the maximum permissible error of the weighing instrument in question
n - is its number of verification scale (*n* = *Max load*/*e*)
e - is the verification scale interval

Only in case that gravity zones are defined in the respective country and if the weighing instrument is marked with gravity zone the user is allowed to freely move his instrument in this particular zone without making the verification invalid.

4. CONCLUSIONS

The method of the absolute gravity measurement and the absolute gravimeter IMGC-02 developed in INRIM are reported. Also the experimental results of measurements performed for four days in gravity laboratory of INRIM. In the paper are also presented some applications of gravity measurements:

- *application in comparison between Pt-Ir kilogram and stainless steel mass standards*
- *application in the calibration process of Non Automatic Weighing Instrument*

Measurements were performed in two different places, respectively Tirana and Vlore, which have a distance of about 100 km from each other and a difference in height above sea level approximately 45 m. It is assumed that the difference in indication value before adjustment process is approximately 1.2×10^{-1} g in the maximum load, for the weighing instrument of class II, with interval scale d = 0.01g. It can be seen that, for the same nominal mass, the indication of weighing instrument in Vlore is lower than in Tirana. After the adjustment is performed, this difference is 4.0×10^{-2} g. Therefore the effect and the correction of absolute gravity value for this weighing instrument are very essential.

- *application in the verification process of weighing instrument under legal control*

For the verification process of NAWI the maximum permissible variation $\Delta g/g$ must fulfil the condition (4). In this case, if the adjustment process is not performed before the verification of the weighing instrument, the error of indication of this weighing instrument could lead in incorrect decision of balance performance.

REFERENCES

[1] G.D'Agostino, S. Desogus, A. Germak et al," The new IMGC-02 transportable absolute gravimeter: measurements apparatus and applications in geophysics and volcanology", *Annals of Geophysics*,vol.51.2008

[2] R. Schwartz, M. Borys, F. Scholz, 2007. Braunschweig, Guide to Mass Determination with High Accuracy.*PTB-MA-80e*.

[3] Adriana Valcu, Dumitru Dinu, Ctin Militaru, On the high accurate automatic mass calibration of disc weights from (500…100) g, *Proceedings of International Metrology Conference CAFMET*, 2008

[4] Guidelines on the Calibration of Non-Automatic Weighing Instruments. *EURAMET* Version 04. 11/2015.

[5] Guide on Common application of Directive 2009/23/EC Non-automatic weighing instruments *WELMEC* 2 2015.

Институт за физика

Physica Macedonica **62**, (2016) p. 41-47

GAMMA RADIATION SYNTHESIS OF POLYMERS AND CONTROL OF THE MECHANICHAL PROPERTIES

N. Mahmudi[1] and S. Rendevski[2]

[1]Faculty of Natural Sciences and Mathematics, State University of Tetovo, bul. Ilinden, b.b., 1200 Tetovo, Republic of Macedonia

[2]Faculty of Engineering and Technology, Department of Mathematics and Physics, Higher Colleges of Technology, Ras al Khaimah Men's Campus, United Arab Emirates

Abstract. The gamma radiation from the radiation source Co-60 was used to synthesize various polymers and copolymers of the hydrogel type. Ions and excited molecules are obtained through this radiation which then initiates the polymerization process. The formation of different polymeric networks from the polymeric chains is obtained with the help of gamma radiation, a process which can be controlled through the radiation doses. Different doses of radiation condition the mechanical properties such as the swelling degree of hydrogel in equilibrium and elastic module. The synthesis of polymeric chains from different monomers such as: AAm, MAAm, HEMA and the MBA crosslinker is made with the purpose of obtaining polymers with different properties. The combination of different amounts of monomers and the used crosslinker enables obtaining different polymeric networks with the desired mechanical properties.

PACS: 61.25.hp, 07.85.-m, 61.25.hp,

1. INTRODUCTION

Polymers are formed throughout polymerization of molecules from which are built constituent elements-monomer units. In the literature are described two techniques used for polymerization: the polymerization with the help of free radicals (addition and chain polymerization) and condensation polymerization, first time proposed from Carothers at 1929 [1-3]. Very often were used synonyms condensation polymerizations and addition or chain polymerization because this classification of Carothers is based on the mechanisms of polymerization processes. Addition polymers are formed with chain polymerization whereas condensation polymers with gradually polymerization. Condensation polymers are those polymers which are formed from poly functional monomers with different condensation reactions of organic compound with elimination of small molecules such as water. Many hydrogels used in medicine such as PHEMA or copolymers such as 2-hydroxyethyl methacrylate with methacrylic acid or N-isopropyl acrylamide with acrylic acid and others [4,5], are synthesized with polymerization with free radicals whereas hydrogels used for controlled release of different substances in agriculture are synthesized with gamma radiation [1,6]. But exists many synthesized and modified hydrogels with the help of gamma radiation which are used in medicine, [8].

Crosslinking with gamma radiation commercial application found in the crosslinking of polyethylene, PVC for wires and isolation of power cords and different package films, separation processes and other applications. Mono functional and multi functional molecules from which are built monomers are mixed together and polymerization begins by adding small molecules named initiators. Polymerization reaction is initiated from free radicals generated from some thermal, ionization, radiation or redox initiator [1]. Gamma radiation also can be used as initiator of polymerization reaction because from their action are produced radical molecules which serves as initiators [2,3]. This method has many advantages in comparison with chemical methods in sense of creation of relatively clearly hydrogels, without chemical residues which might be toxic or non desirable because their tending to bind chemically with polymer chains.

Crosslinking of polymers in order to create hydrogel can be achieved with radiation of linear polymers with gamma rays. Crosslinking comes under consideration through reaction between neighboring chains with the help of action of gamma rays. Polyacrylamides, polyacrylates and polyvinyl alcohol are some of hydrophilic polymers which can be crosslinked with gamma radiation [8-13]. Polymerization involves at least three special stages: chain initiation, chain propagation and chain termination of polymerization. After that, the obtained polymer can be modified with further reactions such as chain transfer [14]. Radiation is particularly important in the initial stage, acting as a manner of starting of reaction of production of ions and free radicals, whereas the reaction take place despite of that. The number of growing chains which can react between themselves depend on the intensity of radiation which is of particular importance in the polymerization [1].

The polymerization under radiation can be made in different states of substances: gas, liquid, solid state, solution, emulsion or dispersion. Many polymers, after exposition of small doses of high energy gamma radiation, exhibit increase of viscosity, increase of average molecular weight and degree of branches [15]. These changes comes from the dimerization-mutual crosslinking of molecules. During reaction are formed closed chains and is formed three dimensional polymer network. The properties of this polymeric network are too different from network made from linear or branched polymers.

Elastic properties and shear modulus of hydrogels were determined by using a Zwick Z010 model Universal Testing Instrument and uniaxial compression module. The crosshead speed was 5 mm/min. The mechanical test is important for the determination of the basic parameters that describe the structure of hydrogels, the average molecular weight between cross-links or cross-link density of the network and elastic modulus G of the polymer samples. Several theories have been proposed to calculate the average molecular weight between cross-links. In the highly swollen state, the constrained junction theory indicates that a real network exhibits properties closer to those of the phantom network model [16,17]. In the literature the derived equation from phantom network, known as Flory-Rehner equation, has been used for nonionic polymeric networks for the determination of average molecular weight between cross-links and elastic modulus of the samples [18].

2. EXPERIMENTAL

In this research three components were used in the preparation of acrylamide-methylenebisacrylamide P(AAm/MBA/water) hydrogels, namely acrylamide as a monomers and methylenebisacrylamide as a cross-linking agent, four components for the acrylamide/methacrylamide/methylenebisacrylamide P(AAm/MAAm/MBA/water) hydrogels, namely acrylamide and methacrylamide as a monomers, methylenebisacrylamide as a cross-linking agent and water as a dispersing medium; three components in the preparation of acrylamide-2-hydroxyethyl methacrylate-methylenebisacrylamide P(AAm/HEMA/water) hydrogels, namely acrylamide and 2-hydroxyethyl methacrylate as monomers and water as dispersing medium. The mass/volume proportion of the monomers in the initial mixtures is summarized in the Table 1.

Table 1: Mass composition of monomers and cross-linking agent in the feed solutions and corresponding abbreviations used for the hydrogels

Gel code	Mass of monomers, cross-linking agent and water volume and dose of radiation					
	AAm (g)	MAAm (g)	HEMA (ml)	MBA (mg)	Water (ml)	Dose (kGy)
1AAm	1.0	–	–	–	1	12.9
1AAm	1.0	–	–	–	1	20.1
1AAm	1.0	–	–	–	1	26.2
1AAm0.1MBA	1.0	–	–	0.1	1	6.6
1AAm0.2MBA	1.0	–	–	0.2	1	6.6
1AAm0.4MBA	1.0	–	–	0.4	1	6.6
0.9AAm0.1MAAm2MBA	0.9	0.1	–	2.0	1	5.0
0.9AAm0.1MAAm2MBA	0.9	0.1	–	2.0	1	15.0
0.9AAm0.1MAAm2MBA	0.9	0.1	–	2.0	1	25.0
1AAm1HEMA	1.0	–	1.0	–	2	5.6
1AAm1HEMA	1.0	–	1.0	–	2	25.9
1AAm1HEMA	1.0	–	1.0	–	2	32.4
1AAm0.6HEMA	1.0	–	0.6	–	2	6.4
1AAm0.8HEMA	1.0	–	0.8	–	2	6.4
1AAm1HEMA	1.0	–	1.0	–	2	6.4
1AAm1.5HEMA	1.0	–	1.5	–	2	6.4
1AAm2HEMA	1.0	–	2.0	–	2	6.4
1AAm2.5HEMA	1.0	–	2.5	–	2	6.4

All compositions, AAm/water, AAm/MBA/water, AAm/MAAm/MBA/water and AAm/HEMA/water solutions were placed in PVC straws of 3 mm diameter and irradiated at different doses, as noted in the Table 1. They have been determined to be optimum doses corresponding to complete conversion or to control the mechanical properties of the obtained polymer networks. Fresh hydrogels obtained in long cylindrical shapes were cut into pieces 3-4 mm in length. Unreacted monomers and uncrosslinked polymers were removed by washing the gels for two days in distilled water. They were dried in vacuum oven in 315 K.

3. RESULTS AND DISCUSSION

For the characterization of the network structure and determination of effective cross-link density of prepared hydrogels their swelling behavior at pH 7 was first investigated. The percentage swelling of hydrogels was calculated by the following equation:

$$S\%(m) = \left[\left(m_t - m_o \right) / m_o \right] / 100 \quad (1)$$

where m_t and m_o are the weights of the swollen and dry gels respectively. The % equilibrium swelling values of all prepared hydrogels at corresponding doses were collected in Table 2. As can be seen from the table, different dose condition the equilibrium values of AAm, AAm/MAAm/MBA and AAm/HEMA hydrogels. The increasing irradiation dose contribute to the decreasing of equilibrium values of the corresponding compositions of the polymers, namely from 772% at 12.9 kGy to 709% at 26.1 kGy in the AAm hydrogels; from 491% at 5 kGy to 456% at 25 kGy in the AAm/MAAm/MBA hydrogels or from 484% at 5.6 kGy to 400% at 32.4 kGy in the AAm/HEMA hydrogels. The equilibrium swelling degree can be controlled using different amounts of cross-linking agent MBA. The increased dose of MBA from 0.1mg to 0.4mg decrease the equilibrium swelling values from 550% to 470%. The same equilibrium swelling values can be controlled by changing the amount of the used monomer HEMA in the AAm/HEMA compositions, namely from 794% to 246% changing the amount of HEMA from 0.6 ml to 2.5 ml into AAm/HEMA compositions. The equilibrium value of swelling was used to calculate the volume fraction of polymer (ν_{2m}) by using Eq. (2) given below where ρ and ρ_w are the densities of dry gel and water. *w* is the weight fraction of polymer in swollen gel.

$$\frac{1}{\nu_{2m}} = \left(1 + \frac{\rho}{\rho_m} \right) \left(w^{-1} - 1 \right) \quad (2)$$

For the investigation of the effect of cross-linking agent MBA on the mechanical properties of AAm polymers and monomer HEMA into AAm/HEMA polymers at unchanged irradiated dose of 6.6 kGy and 6.4 kGy respectively, the mechanical test were made. The stress-strain curves obtained for AAm/HEMA polymers are shown in Figure 1 whereas λ-λ^{-2} versus stress curves of AAm/HEMA hydrogels are shown in Figure 2. Here, λ is the deformation ratio and equal to L/L_o. L_o and L are the lengths of the undeformed and deformed hydrogels during compression, respectively.

Table 2: The hydrogels, the used doses and their equilibrium swelling values.

Gel code	Dose (kGy)	S%
1AAm	12.9	772
1AAm	20.1	730
1AAm	26.2	709
1AAm0.1MBA	6.6	550
1AAm0.2MBA	6.6	510
1AAm0.4MBA	6.6	470
0.9AAm0.1MAAm2MBA	5	491
0.9AAm0.1MAAm2MBA	15	481
0.9AAm0.1MAAm2MBA	25	456
1AAm1HEMA	5.6	484
1AAm1HEMA	25.9	472
1AAm1HEMA	32.4	400
1AAm0.6HEMA	6.4	794
1AAm0.8HEMA	6.4	662
1AAm1HEMA	6.4	544
1AAm1.5HEMA	6.4	380
1AAm2HEMA	6.4	301
1AAm2.5HEMA	6.4	246

The G value was calculated from the slope of the lines and listed in Table 3 and Table 4. By using G values and other relevant experimental parameters, $\overline{M}_c$ and ν_e were calculated and collected in Table 3 and Table 4. As can be seen from Table 3, $\overline{M}_c$ and ν_e can be controlled by changing the cross-linking agent MBA. Increasing the amount of MBA from 0.1mg to 0.4mg decrease $\overline{M}_c$ from 33940 g/mol to 33240 g/mol; whereas, from Table 4, changing the amount of the used monomer HEMA into the AAm/HEMA compositions from 0.6 ml to 2.5 ml, cause changing of the $\overline{M}_c$ from 15327 g/mol to 12239 g/mol respectively.

Changing the amount of MBA from 0.1mg to 0.4mg into AAm/MBA compositions cause increase of the G values from 82.9 kPa to 104 kPa and changing the amount of HEMA into the AAm/HEMA compositions from 0.6 ml to 2.5 ml cause the increase of G values from 16.7 kPa to 38.4 kPa. As can be seen from Table 3 and Table 4, the magnitudes of $\overline{M}_{c(m)}$ calculated from mechanical properties are different from those obtained by using swelling experiments $\overline{M}_{c(s)}$ [16]. Large difference was attributed to using incorrect χ parameter in the modified Flory–Rehner equation [17]. The actual χ parameters were calculated by using $\overline{M}_c(m)$ values [17,18]. Recalculated parameters (χ_m) and the differences between χ_s and χ_m are also given in Table 3 and Table 4. For the investigation of the effect of χ parameter on the $\overline{M}_c$ values the theoretical $\overline{M}_c$ values may be obtained by using χ and experimentally obtained polymer based parameter [19]. ρ is the polymer density whereas ν_e is the effective cross-link density of the cross-linked structure obtained from the results of compressive strain measurements [20].

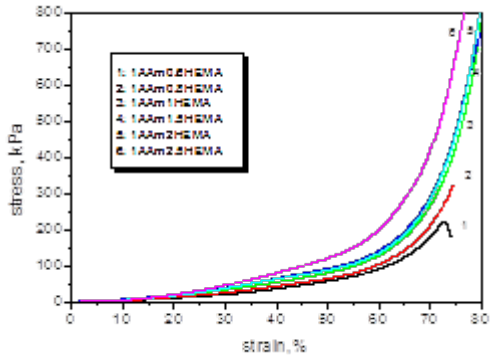

Figure 1. Fig. 1: Strain versus stress curves of AAm/HEMA hydrogels.

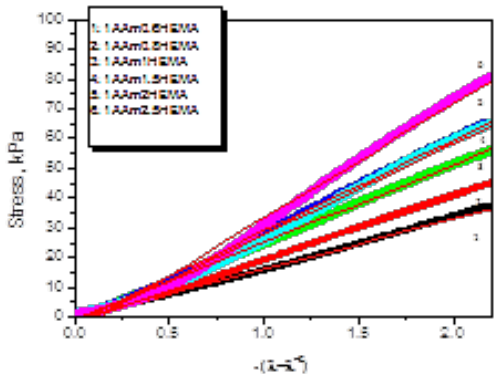

Figure 2. λ-λ^{-2} versus stress curves of AAm/HEMA hydrogels.

Table 3: Network properties and cross-link densities of AAm/MBA hydrogels.

Sample	S(%)	χ_s	$\overline{M}_{c\,(s)}$ (g/mol)	$\overline{M}_{c\,(m)}$ (g/mol)	χ_m	$\nu_{e(s)}$	$\nu_{e(m)}$	χ_s - χ_m	G (kPa)	ν_{2m}	ρ(kg/m^3)
1AAm/0.1MBA	550	0.5409	338435	33940	0.5043	3.39E-05	3.30E-04	0.0366	82.9	0.122684	1303
1AAm/0.2MBA	510	0.5439	229010	33585	0.5095	4.45E-05	3.60E-04	0.0344	91.9	0.131676	1303
1AAm/0.4MBA	470	0.5471	222400	33240	0.5138	5.80E-05	4.00E-04	0.0332	104.0	0.141185	1289

Table 4: Network properties and cross-link densities of AAm/HEMA hydrogels.

Sample	S(%)	χ_s	$\overline{M}_{c\,(s)}$ (g/mol)	$\overline{M}_{c\,(m)}$ (g/mol)	χ_m	$\nu_{e(s)}$	$\nu_{e(m)}$	$\chi_s - \chi_m$	G (kPa)	$_{2m}$	ρ(kg/m^3)
1gAAm/ 0.6ml HEMA/2ml H_2O	794	0.5279	142012	15327	0.5123	9.08E-06	8.42E-05	0.00333	16.7	0.083967	1289.9
1gAAm/ 0.8ml HEMA/2ml H_2O	662	0.5338	72585	13660	0.5217	1.76E-05	9.38E-05	0.00607	20.7	0.10148	1281
1gAAm/ 1ml HEMA/2ml H_2O	544	0.5405	38440	12170	0.5316	3.35E-05	0.000106	0.00515	25.8	0.121582	1285.9
1gAAm/ 1.5ml HEMA/2ml H_2O	380	0.5555	12785	12575	0.5554	0.0001	0.000102	0.00573	30.6	0.16661	1284.8
1gAAm/ 2ml HEMA/2ml H_2O	301	0.5674	6299	13908	0.5741	0,000203	9.17E-05	0.00456	34.6	0.202217	1276.1
1gAAm/ 2.5ml HEMA/2ml H_2O	246	0.5783	3694	12239	0.5902	0,000346	0.000104	000511	38.4	0.234994	1277.4

4. CONCLUSIONS

The aim of this study was to show the ways of control of mechanical properties, equilibrium swelling

values, average molecular weight between cross-links or cross-link density of the network and elastic modulus *G* of the polymer samples. Some of the possible ways to do that are: different amount of the used irradiation dose, different amount of cross-linked agents such as MBA and different amounts of used monomer into polymer compositions. The determination of elastic properties was made by two methods, the swelling method and mechanical test. Comparison of values obtained by these two methods showed large difference between them which is attributed to the incorrect value of the χ parameter used in the modified Flory-Rehner equation. For the reliable determination of cross-link density of hydrogels by swelling experiment the χ parameter must be determined experimentally.

REFERENCES

[1] Odian, G. Principles of polymerization. John Wiley & Sons, New York, (2004)

[2] Krzysztof Matyjaszewski, Thomas P. Davis, Handbook of radical polymerization, A John Wiley & Sons, Inc., New York (2002)

[3] Young, R.J., Lovell, P.A., Introduction to Polymers, Chapman & Hall, Cambridge, (1996)

[4] Peppas, N.A. and Mikos, A.G. Preparation methods and structure of hydrogels. In: N.A. Peppas (Ed.), Hydrogels in Medicine and Pharmacy, Vol. **1**, CRC Press, Boca Raton, FL, pp. 1-27, (1987)

[5] IAEA-TECDOC-1465 Radiation synthesis of stimuli responsive membranes, hydrogels and adsorbents for separation purposes, Viena (2005)

[6] Saraydın, D., Karadağ, E., Güven, O., Polymer Bulletin **41**, 577-584 (1998

[7] IAEA-TECDOC-1324 Radiation synthesis and modification of polymers for med. applications, Viena (2002)

[8] Philipp, B., Dautzenberg, H., Linow, K.-J., Kotz, J. and Dawydoff, W., *Prog. Polym. Sci*. **14**, 91-172 (1989)
[9] Siyam, T., Gamma Radiation Induced Preparation of Polyelectrolytes and Its Use for Treatment of Waste Water, Hot Laboratory Centre, Atomic Authority, Cairo, Egypt
[10] Wang, B., Mukataka, S., Kokufuta, E., Ogiso, M., Kodama, M., *Journal of Polymer Science: Part B*: *Polymer Physics*, Vol.**38**, 214-221 (2000)
[11] Güven, O., Şen, M., *Polymer*, V.**32** N.13, 2491-2496 (1991)
[12] Polymer Data Handbook, Inc, Oxford University Press (1999)
[13] Sperling, L.H., Introduction to Physical Polymer Science, Fourth Edition, John Wiley & Sons, Inc.,. Hoboken, New Jersey (2006)
[14] A. Ravve, Principles of Polymer Chemistry 3rd edition, Springer, New York (2012)
[15] Encyclopedia of Polymer Science and Technology, Radiation Chemistry of Polymers, pdf
[16] W. Xue, S. Champ, M.B. Huglin, Polymer 42 (2001) 3665.
[17] J.E. Mark, B. Erman (Eds.), Rubberlike Elasticity a Molecular Primer, Wiley, New York, 1988.
[18] M. Şen, N. Pekel, O. Güven, Angew. Macromol. Chem. 251 (1998) 1.
[19] N. Mahmudi, M. Şen, S. Rendevski, O. Güven, NIMB in Physics Research B 265 (2007) 375-378.
[20] O. Okay, S. Durmaz, Polymer 43 (2002) 1215.

GENERAL RULES

PHYSICA MACEDONICA is an official publication of the Institute of Physics, Faculty of Natural Sciences and Mathematics, St. Cyril and Methodius University, Skopje, Macedonia, which presents the scientific work of the physicist in the Republic of Macedonia. It's an annual publication. Authentic scientific papers concerning physics are published in **PHYSICA MACEDONICA.**

We would ask the authors of the papers meant for the above-mentioned journal to prepare their papers according to the following recommendations:

The pages of the text should be of the following size: **15x24 cm**, i.e. A4 format the left and the right margins **3 cm**, top and bottom margins **3 cm**, without numeration.

The title: capital letters, font 13 and bold type, and the top margin should be 2 cm lower (4 cm from the top edge of the sheet of paper). **The name and the address**: of the authors: font 12, **the text**: font 11, **subtitles**: capital letters, font 11, bold, not centred, with 1,5 cm indentation, **new lines**: 1,5 cm indentation

The text shouldn't be longer than **8 pages**, typed in **Word with single space**.

The paper is published in **English** with a Macedonian summary. The paper shouldn't have been published. If the methods of work are already published, they shouldn't be repeated, but the authors should cite the previously published papers.

The abstract shouldn't contain more than 150 words and it is differ from the conclusion, font 10, 2 cm indentation.

The recommended size of the pictures is not more than 10 cm height and they should be suitable for good reproduction. There should be place inside the text reserved for the picture according to its size.

The tables are in the text and numbered with Roman numerals.

PACS numbers are recommended.[1]

The references should be cited according to the ordinal number in the text in the following manner: [1] Author, journal, volume (bold), page and in the end the year given in brackets.

The footnotes are to be numbered with Arabic subscriptions and located at the bottom of the same page.

The authors should follow the SI.

The paper is to be submitted in a hard copy, with no mistakes and one copy prepared for a review. The referees are anonymous and their suggestions as well as the suggestions of the Board are submitted to the authors who are to comply with them.

The corrected text is to be returned to the Board no later than 7 days.

The authors should submitted-mail address and telephone number.

The paper is to be sent to the Board and hard copy and one published copy at he following address: Editorial Board of PHYSICA MACEDONICA, Faculty of Natural Sciences and Mathematics. Institute of Physics, Gazi Baba bb. P.O.Box 162, 1000 Skopje, Macedonia.

---

[1] We would be very grateful if you substitute PACS (Physics and Astronomy Classification Sheme) for UDC, according to the last classification of the scientific papers from 1990. Under each abstract there should be Pacs number. For instance: PACS numbers: 42,50.AR refers to a particular field-Statistical Optics and Coherent Theory.

ИНСТРУКЦИИ

PHYSICA MACEDONICA е званична публикација на Институтот за физика при Природно-математичкиот факултет на Универзитетот Св. Кирил и Методиј во Скопје, во која се публикува научната мисла на физичарите на Р. Македонија. Излегува еднаш годишно. Во **PHYSICA MACEDONICA** се печатат оригинални научни трудови од областа на физиката.

Ги молиме авторите, трудовите за печатење во наведениов часопис да ги припремаат според следниве препораки:

Наслов: големи букви, фонт 13 болд, а горната маргина да биде 4 цм подолу (7 цм од горната ивица на листот). **Име и адреса на авторите**: фонт 12, **текст**: фонт 11, **поднаслов**: големи букви, фонт 11 болд, не центрирани 1,5 cm повнатре. **Нов ред**: 1,5 cm повнатре.

Страниците со текст да се пишуваат на А4 формат и не нумерирани. Сите маргини да се 3 cm.

Трудот се печати на **англиски јазик** со резиме на **македонски јазик.**

Трудот да не е објавуван. Методите на работа ако еднаш се објавени да не се повторуваат, но, авторите да се повикуваат на претходно објавените трудови.

За секој труд авторот треба да внесе PACS numbers[1].

Апстрактот да содржи до **150 збора** и да не се повторува со заклучокот, фонт 10**,** 2 cm повнатре**.**

Сликите по можност да не се поголеми од 10 cm и да овозможуваат добра репродукција. Сите слики треба да бидат доставени во посебен фајл.

Табелите да се внесени во текстот и нумерирани со римски броеви.

Референците да се цитираат по реден број во текстот на следниолв начин: [1] Автор, часопис, том(болд), страна и на крај година во заграда.

Фуснотите да се нумерираат со арапски субскрипти и се поставуваат на дното од истата страна.

Авторите да се придржуваат на SI.

Авторите треба да достават: e-mail и FAX.

Трудот може да се достави на дискета или испрати преку email, притоа потребно е да се достави и еден испечатен примерок припремен за рецензија. Рецензентите се анонимни и нивните сугестии како и сугестиите од Редакцијата се доставуваат на авторите кои се должни да постапат според нив.

Трудот може да се испрати преку пошта до Редакцијата на дискета и отпечатен во еден примерок на следнава **адреса**: Редакциски Одбор на PHYSICA MACEDONICA, Природно-математички факултет, Институт за физика, Гази Баба бб. П. Фах 162, 1000 Скопје, Р. Македонија.

---

[1] Ве молиме наместо UDC, според најновата клсификација на научните трудови од 1990 година, да стои PACS (Physics and Astronomy Classification Sheme). Под секој апстракт да стои PACS numbers. На пример, PACS numbers:42.50.Ar се однесува на областа Статистичка оптика и кохерентна теорија.